



Complex Modulation of Rapidly Rotating Young M Dwarfs: Adding Pieces to the Puzzle

Maximilian N. Günther^{1,2,24} , David A. Berardo¹ , Elsa Ducrot³ , Catriona A. Murray⁴ , Keivan G. Stassun⁵ , Katalin Olah⁶ , L. G. Bouma⁷ , Saul Rappaport¹ , Joshua N. Winn⁷ , Adina D. Feinstein^{8,25} , Elisabeth C. Matthews¹ , Daniel Sebastian³ , Benjamin V. Rackham^{1,9,26} , Bálint Seli⁶ , Amaury H. M. J. Triaud¹⁰ , Edward Gillen^{4,11,27} , Alan M. Levine¹ , Brice-Olivier Demory¹² , Michaël Gillon³ , Didier Queloz^{4,13} , George R. Ricker¹ , Roland K. Vanderspek¹ , Sara Seager^{1,9,14} , David W. Latham¹⁵ , Jon M. Jenkins¹⁶ , C. E. Brasseur¹⁷ , Knicole D. Colón¹⁸ , Tansu Daylan^{1,28} , Laetitia Delrez^{3,13,19} , Michael Fausnaugh¹ , Lionel J. Garcia³ , Rahul Jayaraman¹ , Emmanuel Jehin¹⁹ , Martti H. Kristiansen^{20,21} , J. M. Diederik Kruijssen²² , Peter Pihlmann Pedersen⁴ , Francisco J. Pozuelos^{3,19} , Joseph E. Rodriguez¹⁵ , Bill Wohler²³ , and Zhuchang Zhan⁹

¹ Department of Physics, and Kavli Institute for Astrophysics and Space Research, MIT, 77 Massachusetts Avenue, Cambridge, MA 02139, USA
maximilian.guenther@esa.int

² European Space Agency (ESA), European Space Research and Technology Centre (ESTEC), Keplerlaan 1, 2201 AZ Noordwijk, Netherlands

³ Astrobiology Research Unit, Université de Liège, 19C Allée du 6 Août, B-4000 Liège, Belgium

⁴ Cavendish Laboratory, JJ Thomson Avenue, Cambridge CB3 0HE, UK

⁵ Department of Physics and Astronomy, Vanderbilt University, Nashville, TN 37235, USA

⁶ Konkoly Observatory, Research Centre for Astronomy and Earth Sciences, Hungary

⁷ Department of Astrophysical Sciences, Princeton University, 4 Ivy Lane, Princeton, NJ 08544, USA

⁸ Department of Astronomy and Astrophysics, University of Chicago, 5640 S. Ellis Avenue, Chicago, IL 60637, USA

⁹ Department of Earth, Atmospheric and Planetary Sciences, MIT, 77 Massachusetts Avenue, Cambridge, MA 02139, USA

¹⁰ School of Physics & Astronomy, University of Birmingham, Edgbaston, Birmingham B15 2TT, UK

¹¹ Astronomy Unit, Queen Mary University of London, Mile End Road, London E1 4NS, UK

¹² University of Bern, Center for Space and Habitability, Bern, Switzerland

¹³ Observatoire astronomique de l'Université de Genève, 51 chemin de Pégase, 1290 Sauverny, Switzerland

¹⁴ Department of Aeronautics and Astronautics, MIT, 77 Massachusetts Avenue, Cambridge, MA 02139, USA

¹⁵ Center for Astrophysics | Harvard & Smithsonian, 60 Garden Street, Cambridge, MA 02138, USA

¹⁶ NASA Ames Research Center, Moffett Field, CA 94035, USA

¹⁷ Mikulski Archive for Space Telescopes, USA

¹⁸ NASA Goddard Space Flight Center, Exoplanets and Stellar Astrophysics Laboratory (Code 667), Greenbelt, MD 20771, USA

¹⁹ Space Sciences, Technologies and Astrophysics Research (STAR) Institute, Université de Liège, 19C Allée du 6 Août, B-4000 Liège, Belgium

²⁰ Brorfelde Observatory, Observator Gyldenkerne Vej 7, DK-4340 Tølløse, Denmark

²¹ DTU Space, National Space Institute, Technical University of Denmark, Elektrovej 327, DK-2800 Lyngby, Denmark

²² Astronomisches Rechen-Institut, Zentrum für Astronomie der Universität Heidelberg, Mönchhofstraße 12-14, D-69120 Heidelberg, Germany

²³ SETI Institute/NASA Ames Research Center, USA

Received 2020 August 26; revised 2022 January 25; accepted 2022 January 26; published 2022 March 2

Abstract

New sets of young M dwarfs with complex, sharp-peaked, and strictly periodic photometric modulations have recently been discovered with Kepler/K2 (scallop shells) and TESS (complex rotators). All are part of star-forming associations, are distinct from other variable stars, and likely belong to a unified class. Suggested hypotheses include starspots, accreting dust disks, corotating clouds of material, magnetically constrained material, spots and misaligned disks, and pulsations. Here, we provide a comprehensive overview and add new observational constraints with TESS and SPECULOOS Southern Observatory photometry. We scrutinize all hypotheses from three new angles: (1) We investigate each scenario's occurrence rates via young star catalogs, (2) we study the feature's longevity using over one year of combined data, and (3) we probe the expected color dependency with multicolor photometry. In this process, we also revisit the stellar parameters accounting for activity effects, study stellar flares as activity indicators over year-long timescales, and develop toy models to simulate typical morphologies. We rule out most hypotheses, and only (i) corotating material clouds and (ii) spots and misaligned disks remain feasible—with caveats. For (i), corotating dust might not be stable enough, while corotating gas alone likely cannot cause percentage-scale features and (ii) would require misaligned disks around most young M dwarfs. We thus suggest a unified hypothesis, a superposition of large-amplitude spot modulations and sharp transits of corotating gas clouds. While the complex rotators' mystery remains, these new observations add valuable pieces to the puzzle going forward.

²⁴ Juan Carlos Torres Fellow, ESA Research Fellow.

²⁵ NSF Graduate Research Fellow.

²⁶ 51 Pegasi b Fellow.

²⁷ Winton Fellow.

²⁸ Kavli Fellow.

Unified Astronomy Thesaurus concepts: Variable stars (1761); Periodic variable stars (1213); T Tauri stars (1681); Pre-main sequence stars (1290); M dwarf stars (982); Stellar rotation (1629); Starspots (1572); Stellar activity (1580); Stellar flares (1603)

1. Introduction

1.1. Morphologies of Young M Dwarfs

Young M-dwarf stars (here 20–150 Myr) are often fast rotators, with rotational periods ranging from hours to one or two days. Their rotation is one of the drivers of their magnetic dynamos and thus stellar activity (e.g., Moffatt 1978; Parker 1979; Browning 2008). This can be observed in terms of activity indicators, such as hydrogen and calcium H & K emission lines, frequent and strong flaring activity, and significant starspot coverage (e.g., Benz & Güdel 2010; West et al. 2015; Newton et al. 2017; Wright et al. 2018; Günther et al. 2020).

In photometric observations, young M dwarfs with spots often show smooth, semisinusoidal rotational modulation with amplitudes of a few percent. Their patterns are rather “simple,” manifesting only a few peaks in a Fourier transform, even in the presence of multiple spots and differential rotation (Figure 1 first row). Thus, even the most extreme rotational modulations discovered so far can be described by just a handful of spots (e.g., Rappaport et al. 2014; Strassmeier et al. 2017).

One of the first phenomena clearly standing out from this norm was dipper and burster stars. These show abrupt dips or bursts of light in a quasi-periodic or stochastic manner (Alencar et al. 2010; Morales-Calderón et al. 2011; Cody et al. 2014; Ansdell et al. 2016; Figure 1, second row) and were grouped by their photometric morphology into seven distinct classes.²⁹

Shortly after, Stauffer et al. (2017, 2018) discovered yet again three new morphology classes in Kepler/K2 data.³⁰ As these three share common features, we refer to them collectively as scallop shells throughout this paper (Figure 1 third row). These scallop shells differ from the dippers/bursters in two substantial ways: (1) the objects discussed by Stauffer et al. (2018) are strictly periodic, and (2) they rotate much more rapidly, typically on timescales of $\lesssim 2$ days, compared to the timescales of multiple days to weeks for the dippers/bursters.

Most recently, Zhan et al. (2019) discovered 10 very similar objects in TESS Sectors 1 and 2, dubbed complex rotators (Figure 1, fourth row; see also Figure A1 for a collage of all light curves per TESS orbit). All complex rotators and scallop shells show rapid rotation, strict periodicity, and dozens of harmonics in their frequency spectra indicating their sharp light-curve features. We thus argue that they are likely the same class of objects, and any differences are only due to Kepler’s and TESS’ observing cadences (30 minutes versus 2 minutes). This makes them strictly distinct from “normal” spotted stars (even those with differential rotation), which only show one or two peaks in their frequency spectra, and from dippers, which are far less periodic and morphological stable.

1.2. Hypotheses for Complex Modulations and Their Limitations

All dipper and burster classes were linked to the presence of dusty disks and a viewing-angle dependency, suggested by

observations of strong infrared excess (accreting dust disks; Bodman et al. 2016, Figure 2, first panel).

The scallop shells were first suggested to arise from a patchy torus of material clouds at the Keplerian corotation radius periodically transiting the star (corotating clouds; Stauffer et al. 2017, 2018; Figure 2 second panel).³¹ Such material might be warm coronal gas, dust, or a mixture of both.

When studying the complex rotators, however, Zhan et al. (2019) suggested a new idea: spotted, rapidly rotating stars that host an inner dust disk at a few stellar radii and show a spin-orbit misalignment between their rotation axis and the dust ring (spots and misaligned disk; Figure 2 third panel). Spots might then pass behind the dust disk and get (partially) occulted, leading to sudden increases in photometric brightness.

In particular, Zhan et al. (2019) presented the following counterarguments to the previous hypotheses:

1. *Spots only*: even the superposition of multiple cold and hot stellar spots leads to smooth variations and can only explain one to two peaks in the frequency spectrum (also Kóvári & Bartus 1997; Stauffer et al. 2017).
2. *Accreting dust disk*: (i) the complex rotators’ stable periodicity is in stark contrast to the semiperiodic and stochastic nature of morphologies caused by accreting disks, (ii) the absence of significant infrared excess in their spectral energy distributions (SEDs) contradicts the presence of accreting disks, and (iii) their rotation periods are much shorter than those of dippers (also Stauffer et al. 2017).
3. *Corotating clouds*: (i) if the material is gas, it is challenging to explain the large amplitudes of the modulation; (ii) the material cannot be dust, as it cannot be stably confined at the required distances of several stellar radii because the magnetic field at those large distances from the surface would be too weak; (iii) any material (be it gas or dust) trapped in the magnetic field closer to the stellar surface could not reproduce the observations of sharp features with amplitudes of several percent.

1.3. This Paper

This paper focuses on the 10 targets discovered by Zhan et al. (2019) to further scrutinize the plausibility of several hypotheses by three means:

1. investigating their occurrence rates,
2. studying the morphologies’ stability and longevity over one (noncontinuous) year, and
3. probing the feature’s chromaticity.

We give an overview of all observations in Section 2 and revise the stellar parameters in Section 3. Then, we study stellar flares and other brightenings in Section 4. Next, we scrutinize all hypotheses with respect to occurrence rates, stability and longevity, and color dependency in Section 5. Finally, we discuss our findings and present our conclusion in Sections 6 and 7.

²⁹ Periodic dippers, aperiodic dippers, stochastic variables, periodic variables (likely spots), quasi-periodic variables, bursters, and long-timescale variables.

³⁰ Scallop shell, persistent flux-dip, and narrow flux-dip variables.

³¹ Yu et al. (2015) and Bouma et al. (2020) suggested a similar explanation for the T Tauri star PTFO 8-8695b.

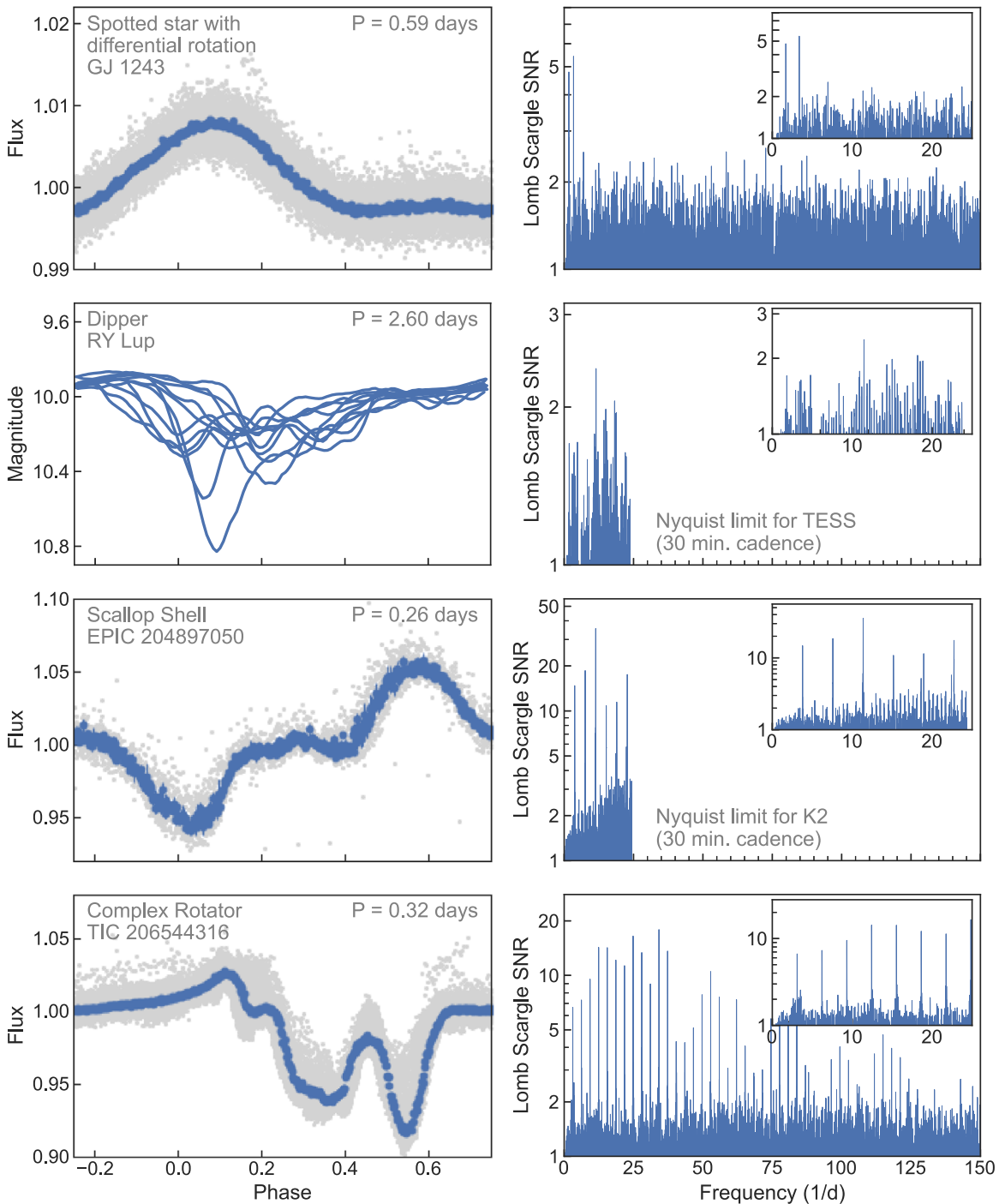


Figure 1. A collage of different morphology classes of young M dwarfs with complex photometric variability. First row: a typical complex rotator (TIC 206544316) with a period of 0.32 days. Its phase-folded light curve highlights the complex modulation, and its frequency spectrum shows dozens of harmonics down to timescales of minutes. Second row: a typical scallop shell (EPIC 204897050) with a period of 0.26 days. It is apparent that these targets share the same morphology class as the complex rotators, even though the data are constrained by the Nyquist limit for K2 (30 minutes cadence). Third row: a typical spotted M dwarf with a period of 0.58 days (GJ 1243; see, e.g., Davenport et al. 2015; Günther & Daylan 2021; Davenport et al. 2020), showing a simple modulation and only two peaks in the frequency spectrum (two peaks rather than one due to differential rotation). Fourth row: a typical dipper star observed with TESS (RY Lup; Bredal et al. 2020), usually showing no strict periodicity, no presence of multiple clear harmonics, and a wider range of periods (multiple days to weeks). Not shown are the more standard variability classes, such as single-spot modulation and binary stars.

2. Observations

2.1. TESS Photometry

The 10 complex rotators were discovered in TESS short-cadence data from Sector 1 (2018 July 25 to 2018 August 22) and Sector 2 (2018 August 22 to 2018 September 10) and

observed as part of the cool dwarf catalog (Muirhead et al. 2018; Stassun et al. 2018). Here, we also add new data taken over the full first year of operations (Table 1). Light curves were prepared with the Science Processing Operations Center (SPOC) pipeline (Jenkins et al. 2016), a descendant of the Kepler mission pipeline (Jenkins 2002; Jenkins et al. 2010;

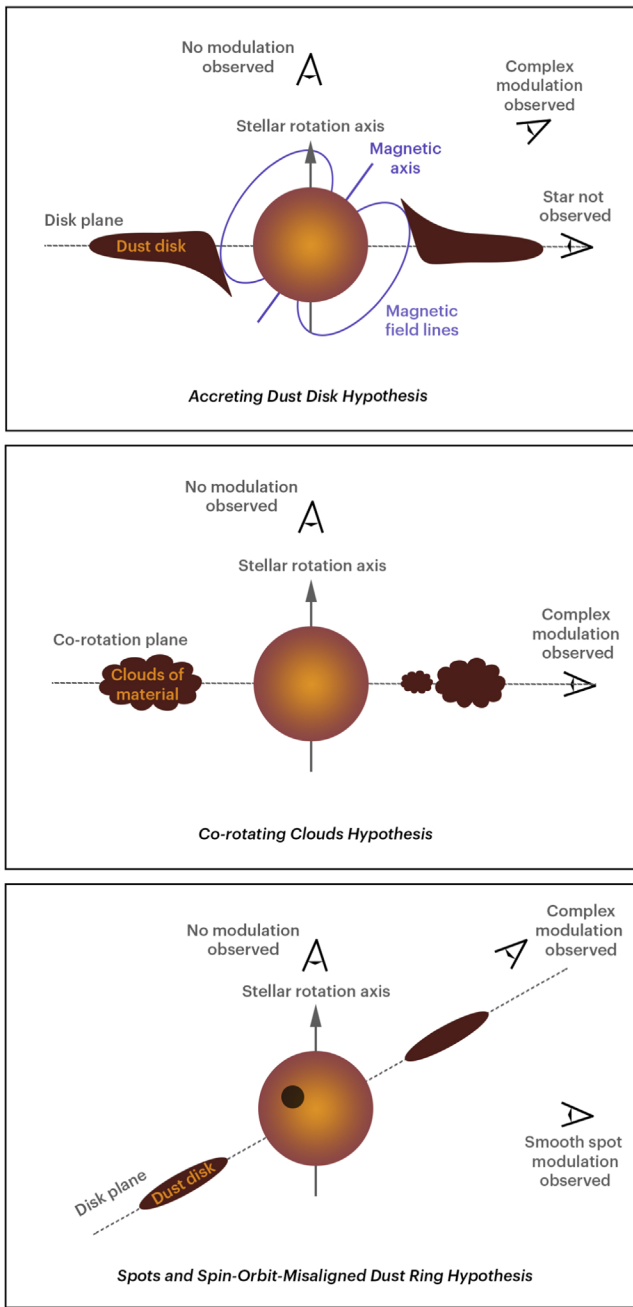


Figure 2. Three hypotheses to explain complex morphologies of young M dwarfs. First panel: accreting dust disk hypothesis (Bodman et al. 2016), where an accreting dust disk seen from different observing angles could explain dipper and burster stars. Second panel: corotating clouds hypothesis (Stauffer et al. 2017, 2018), where a patchy torus of gas clouds at the Keplerian corotation orbit periodically blocks out stellar light and might cause scallop shell modulation. Third panel: spots and misaligned disk hypothesis (Zhan et al. 2019), where spot occultations might explain the complex rotator’s modulation.

Smith et al. 2012; Stumpe et al. 2014; Jenkins 2017). We use the presearch data conditioned simple aperture (PDC-SAP) light curves, which are detrended for instrumental systematics.

2.2. SPECULOOS Southern Observatory Photometry

The SPECULOOS Southern Observatory (SSO; Burdanov et al. 2018; Delrez et al. 2018; Gillon 2018) is located at ESO’s Paranal Observatory in Chile and is part of the SPECULOOS

network. The facility consists of four robotic 1 m telescopes (Callisto, Europa, Ganymede, and Io), each equipped with a near-infrared-sensitive CCD camera with a resolution of $0''.35$ per pixel. We observed four targets, TIC 201789285, TIC 206544316, TIC 332517282, and TIC 425933644, each simultaneously in at least two wavelength bands (g' -, r' -, i' -, and z' -band filters) for an entire observing night (Table A1). We extracted light curves using the SSO pipeline (Murray et al. 2020), which uses the `casutools` software (Irwin et al. 2004) for automated differential photometry and detrends for telluric water vapor.

2.3. ANU Spectroscopy

We also reuse the spectroscopic observations taken by Zhan et al. (2019). The low-resolution spectra covered four of the systems (TIC 177309964, TIC 206544316, TIC 234295610, and TIC 425933644) using the Wide Field Spectrograph (WiFeS; Dopita et al. 2007) on the Australian National University (ANU) 2.3 m telescope at Siding Spring Observatory, Australia, on 2019 January 18 and 19. The observations cover the 5200–7000 Å band with a resolving power of $R = 7000$ and were reduced following Bayliss et al. (2013). All spectra reveal strong $H\alpha$ emission features with equivalent widths (EWs) of 4–7 Å, typical of rapidly rotating young M stars (see Section 3). No signs of the binary nature of these four objects were found.

3. Revising the Stellar Parameters

3.1. Revisiting the Binary TIC 289840928 and TIC 289840926

Zhan et al. (2019) found two prominent rotation periods for TIC 289840928, which is in a spatially resolved binary system with TIC 289840926, and both stars are blended in a single TESS pixel. In our reanalysis, the TESS pixel-level data revealed the primary (TIC 289840928, M4V, 3100 K) only has a smooth spot modulation with a period of 15.625 hr, while the secondary (TIC 289840926, M6V, 2800 K) is the actual complex rotator with 2.400 hr. We thus update all corresponding values here.

3.2. Ages and Activity Corrections

Zhan et al. (2019) estimated the ages of all 10 complex rotators via their probabilistic membership of young stellar associations, using the `banyan sigma` software (Gagné et al. 2018), with input from the TESS Input Catalog version 8 (TICv8; Stassun et al. 2018) and Gaia Data Release 2 (Gaia DR2 Gaia Collaboration et al. 2018). They found that all 10 targets have a high probability of belonging to young associations (see Table 1).³²

We here conduct an independent estimate of their stellar age. Young M dwarfs are pre-main-sequence stars and as such have larger radii than their main-sequence counterparts of the same mass. Additionally, they have high levels of activity, leading to activity-induced radius inflation and temperature suppression (Stassun et al. 2012). This could be due to strong chromospheric activity, presumably arising from rapid rotation. We can thus use the ANU spectra of four targets (Section 2.3) to explore if these stars have larger radii than expected for the main sequence.

For example, TIC 234295610 shows a $H\alpha$ EW of 6.8 Å in the ANU spectrum. According to the empirical relations from

³² There seems to be a typo in Zhan et al. (2019), as TIC 206544316 is a member of Tucana Horologium (not of AB Doradus).

Table 1
Updated Parameters of the Complex Rotators from TESS Sectors 1 and 2

TIC ID ¹	38820496	177309964	201789285	206544316	224283342	234295610	289840926*	332517282	425933644	425937691
R.A. (deg) ¹	7.19516	103.45258	33.88868	18.41884	356.35758	357.98325	317.629044	350.8786	3.69942	5.36556
Decl. (deg) ¹	-67.86237	-75.70396	-56.45488	-59.65974	-40.33782	-64.79293	-27.18098	-28.12114	-60.06352	-63.85226
Association ²	Tuc. Hor.	Carina	Tuc. Hor.	Tuc. Hor.	Columba	Tuc. Hor.	β Pictoris	AB Doradus	Tuc. Hor.	Tuc. Hor.
Membership Probability ²	99.9%	83.2%	99.7%	100.0%	75.0%	99.9%	99.0%	99.1%	99.8%	98.8%
Age (Myr) ²	45 \pm 4	45 ⁺¹¹ ₋₇	45 \pm 4	45 \pm 4	42 ⁺⁶ ₋₄	45 \pm 4	24 \pm 3	149 ⁺⁵¹ ₋₁₀	45 \pm 4	45 \pm 4
Distance (pc) ¹	44.06 \pm 0.12	91.08 \pm 0.49	45.16 \pm 0.17	43.07 \pm 0.10	38.12 \pm 0.10	48.17 \pm 0.11	40.33 \pm 0.18	39.08 \pm 0.10	44.26 \pm 0.18	-
Rotation Period (h) ³	15.71	10.88	3.64	7.73	21.35	18.28	2.40	9.67	11.67	4.82
H α Equivalent Width (Å) ⁴	(5.3)	5.8	(5.3)	4.8	(5.3)	6.8	(5.3)	(5.3)	3.8	(5.3)
App. Eff. Temp., $T_{\text{eff}}^{\text{app}}$ (K) ⁵	3000 \pm 100	3200 \pm 100	2800 \pm 100	3100 \pm 100	3100 \pm 100	3100 \pm 100	2700 \pm 100	3000 \pm 100	3200 \pm 100	2800 \pm 100
App. Radius, R_{\star}^{app} (R_{\odot}) ⁵	0.30 \pm 0.02	0.57 \pm 0.04	0.27 \pm 0.02	0.54 \pm 0.04	0.36 \pm 0.02	0.42 \pm 0.03	0.38 \pm 0.03	0.27 \pm 0.02	0.59 \pm 0.04	0.38 \pm 0.03
Temp. Suppression ⁶	(6.2%)	6.5%	(6.2%)	6%	(6.2%)	7.1%	(6.2%)	(6.2%)	5.3%	(6.2%)
Radius Inflation ⁶	(13.5%)	14%	(13.5%)	13%	(13.5%)	15.6%	(13.5%)	(13.5%)	11.5%	(13.5%)
Eff. Temp., $T_{\text{eff}}^{\text{w/o act}}$ (K) ⁶	(3200)	3400 \pm 100	(3000)	3300 \pm 100	(3300)	3300 \pm 100	(2800)	(3200)	3400 \pm 100	(3000)
Radius, $R_{\star}^{\text{w/o act}}$ (R_{\odot}) ⁶	(0.26)	0.50 \pm 0.04	(0.24)	0.48 \pm 0.04	(0.32)	0.36 \pm 0.03	(0.33)	(0.23)	0.53 \pm 0.04	(0.33)
Mass, M_{\star} (M_{\odot}) ⁷	(0.15)	0.29	(0.08)	0.22	(0.19)	0.2	(0.08)	(0.16)	0.29	(0.08)
Surface Gravity, $\log_{10}(g)$	(4.7)	4.4	(4.5)	4.3	(4.6)	4.5	(4.2)	(4.8)	4.4	(4.2)
Corotation Radius, R_{cr} (R_{\star})	5.6	2.9	1.9	2.2	6.2	4.9	1.0	4.6	2.9	1.6
TESS Sectors	1–2	1–13	2–3	1–2	2	1	1	2	1–2	1–2

Note. Tuc. Hor.: Tucana Horologium. (1) from TICv8 (Stassun et al. 2018); (2) via Banyan Sigma (Gagné et al. 2018); (3) via TESS photometry; (4) via ANU spectroscopy; (5) via SED fit; (6) via (Stassun et al. 2012); (7) via the Baraffe et al. (2015) models for a star with the respective age, $T_{\text{eff}}^{\text{w/o act}}$, and $R_{\star}^{\text{w/o act}}$. Values in parentheses are only estimated using the mean H α EW of the other four targets and should only be used as approximate guidance. * TIC 289840926 and TIC 289840928 form a binary system that is blended in a single TESS pixel but is spatially resolved by other surveys. TIC 289840926 is the complex rotator (see Section 3.1).

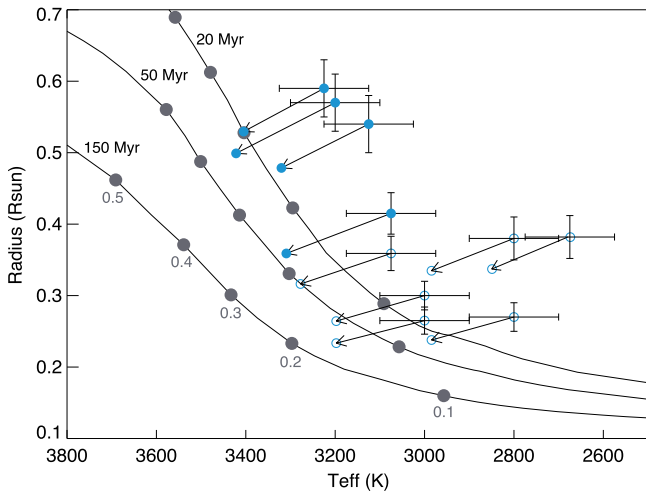


Figure 3. Revised stellar parameters of the 10 complex rotators after correcting for activity-induced radius inflation and temperature suppression. Solid curves are isochrones from the Baraffe et al. (2015) models for ages of 20, 50, and 150 Myr, with gray circles marking masses at $0.1 M_{\odot}$ increments. Error bars show apparent effective temperatures (T_{eff}) and radii measured from SED analyses. Arrows show where the stars would fall if they were inactive, i.e., after they are corrected for activity. Filled blue circles mark the four targets with $H\alpha$ measurements from ANU (Section 2.3), whereas empty blue circles mark the remaining six targets for which we provide estimates only. The “corrected” values place most of the stars near isochrones consistent with the respective ages estimated from their young association memberships, suggesting inferred masses of $0.1\text{--}0.3 M_{\odot}$ (Table 1).

Stassun et al. (2012), this EW predicts a radius inflation of 15.6% and a temperature suppression of 7.1%. Next, we performed an SED fit to better constrain the apparent radius to $R_{\star}^{\text{apparent}} = 0.415 \pm 0.029 R_{\odot}$ and the apparent temperature to $T_{\text{eff}}^{\text{apparent}} = 3075 \pm 100$ K (see Figure A2). Assuming that this radius and temperature represent the activity-inflated radius and activity-suppressed temperature values, then in the absence of activity, we would have $R_{\star}^{\text{w/o activity}} \approx 0.36 R_{\odot}$ and $T_{\text{eff}}^{\text{w/o activity}} \approx 3300$ K.

Comparing the corrected values with models for low-mass pre-main-sequence stars (Baraffe et al. 2015), we find that they are fully consistent with a star of mass of $0.20 M_{\odot}$ and age of 40 Myr.³³ This leads to a stellar mass that is only half of the mass of a main-sequence star with the same radius and effective temperature. We consider this a strong affirmation of the young age suspected from its young association membership.

We perform the same revision of stellar parameters for all systems. First, we perform SED fits to refine all their $T_{\text{eff}}^{\text{apparent}}$ and $R_{\star}^{\text{apparent}}$ (see Figure A2). Next, for those with ANU spectra (TIC 177309964, TIC 206544316, TIC 234295610, and TIC 425933644), we measure their $H\alpha$ EWs and use them to compute the temperature suppression and radius inflation factors, providing the corresponding values “without activity.” For the other six targets, we provide provisional corrections assuming they have $H\alpha$ EWs comparable to the average of the four measured ANU spectra.

Figure 3 and Table 1 summarize the revised stellar parameters and their isochrone matches. The “corrected” T_{eff} and radii place 9 of the 10 complex rotators in the range of ~ 20 or ~ 50 Myr, consistent with the respective ages of their young associations. Only TIC 332517282 falls closer to the ~ 150 Myr isochrone,

³³ Models from Baraffe et al. (2015) are for stars without activity effects, hence we compare them with our “corrected” values.

consistent with its membership in AB Doradus (150 Myr), making it our single “oldest” star.

4. Flares and Sudden Brightenings

The complex rotators and scallop shells show frequent and large-amplitude flaring, along with other sudden brightenings whose shapes are distinct from usual M-dwarf flare profiles (Stauffer et al. 2017, 2018; Zhan et al. 2019). In particular, brightenings of the entire modulation often appeared right after strong flares, sometimes even followed by changes in the overall morphology, underlining strong magnetic activity.

It is still disputed whether flares on stars other than our Sun correlate with the rotational phase and are linked to localized clusters of spots on the stellar surface. Many previous studies found that superflares were distributed randomly uniform over the rotational phase for main-sequence dwarfs (Doyle et al. 2018; Roettenbacher & Vida 2018; Doyle et al. 2019, 2020) and young stars (Vida et al. 2016; Feinstein et al. 2020b). Doyle et al. (2018) reason that depending on the viewing geometry, polar spots could be seen at all phases, and their interaction with emerging active regions can thus cause continuously visible flaring. However, other studies found flares to be more prominent at certain rotational phases and hence potentially bound to the locations of starspots for the Sun (Zhang et al. 2008), Sun-like stars (Notsu et al. 2013), and the smallest flares on main-sequence dwarfs (Roettenbacher & Vida 2018). Hence, a unifying idea is that superflares occur over the entire surface while small flares are tied to spots.

Here, we utilize the extended coverage by TESS (up to 1 yr for TIC 177309964) to study whether complex rotators’ flares and other brightenings correlate with the phase of the modulation. We searched the light curves in two ways. In the first approach, we ran the *stella* software, a convolutional neural network developed for probabilistic flare detection in TESS 2 minute cadence data (Feinstein et al. 2020a, 2020b). As the algorithm was trained on a large sample of stars with smooth spot modulation, many of the initial flare candidates were misidentified (often spikes of the complex rotators). By visually vetting, we then selected reliable criteria of a probability ≥ 0.9 and amplitude $\geq 5\%$ and identify a confirmed sample of at least 67 flares on TIC 177309964. In the second approach, we independently inspected the entire light curve by eye and found a total of ~ 70 confirmed flares, agreeing with the machine-learning results.

We find that flares on the complex rotators are distributed randomly uniform in phase, showing no clear dependency of their location or amplitude (see the example of TIC 177309964 in Figure 4). There is also no clear correlation between flare amplitudes and the 1 yr time span. It is peculiar that the three largest flares (amplitudes of 1.5–4 in normalized flux) all occur within two few weeks from one another, but the sample size is too low to rule out mere coincidence. Most flares are described by the same profiles as their main-sequence counterparts, suggesting similar origins and processes driving them. We also observed somewhat more complicated “outbursts” of flares, which again resemble those of main-sequence M dwarfs; these can be explained as superpositions of multiple flare events (e.g., Günther et al. 2020).

Finally, we also find that some sudden brightenings do not resemble typical M-dwarf flare profiles (Figure 5); instead, they seem like amplified versions of the complex periodic morphologies. This was also pointed out in Zhan et al. (2019) and

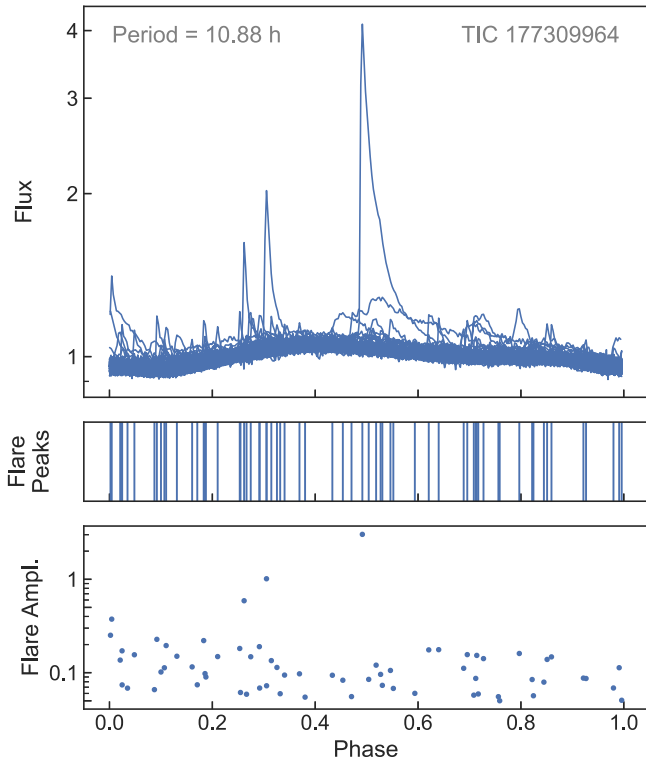


Figure 4. Flares on complex rotators appear randomly uniform distributed in phase, exemplified by 1 yr of TESS data on TIC 177309964. The top panel shows the phase-folded light curve with all flares. The middle panel shows the locations of all flare peaks, illustrating the randomly uniform distribution. The bottom panel illustrates that there is no clear correlation between flare amplitude and phase.

Stauffer et al. (2017), often (but not always) following superflares. On TIC 177309964, these alterations also occur without any preceding flare observation. It is possible that they were triggered by a superflare that was (i) not visible in the visual, but would have been classified as such in the UV or X-ray spectrum (e.g., Wolter et al. 2007; Loyd et al. 2020), or (ii) located outside of the visible hemisphere.

5. Testing the Hypotheses

The limitations of previous hypotheses leave us with two remaining possibilities for the complex rotators and scallop shells: (i) the idea of a patchy torus of clouds of gas at the Keplerian corotation radius (corotating clouds hypothesis) and (ii) the idea of spots being periodically occulted behind a spin-orbit-misaligned dust disk (spots and misaligned disk hypothesis). In the following analyses, we hence focus on these two cases.

5.1. Occurrence Rates

We can estimate the expected yield of complex rotators in TESS Sectors 1 and 2 from the corotating clouds and spots and misaligned disk hypotheses (see Figure 2), respectively, as

$$N_{\text{comp. rot.}}^{\text{CC}} = N_{\text{yMrr}} \cdot P_{\text{clouds}} \cdot P_{\text{geom}} \quad (1)$$

and

$$N_{\text{comp. rot.}}^{\text{SMD}} = N_{\text{yMrr}} \cdot P_{\text{spots}} \cdot P_{\text{disk}} \cdot P_{\text{misal}} \cdot P_{\text{geom}}. \quad (2)$$

Here, N_{yMrr} is the number of young M dwarfs with rapid rotations ($\lesssim 2$ days), which were observed by TESS in short-cadence mode

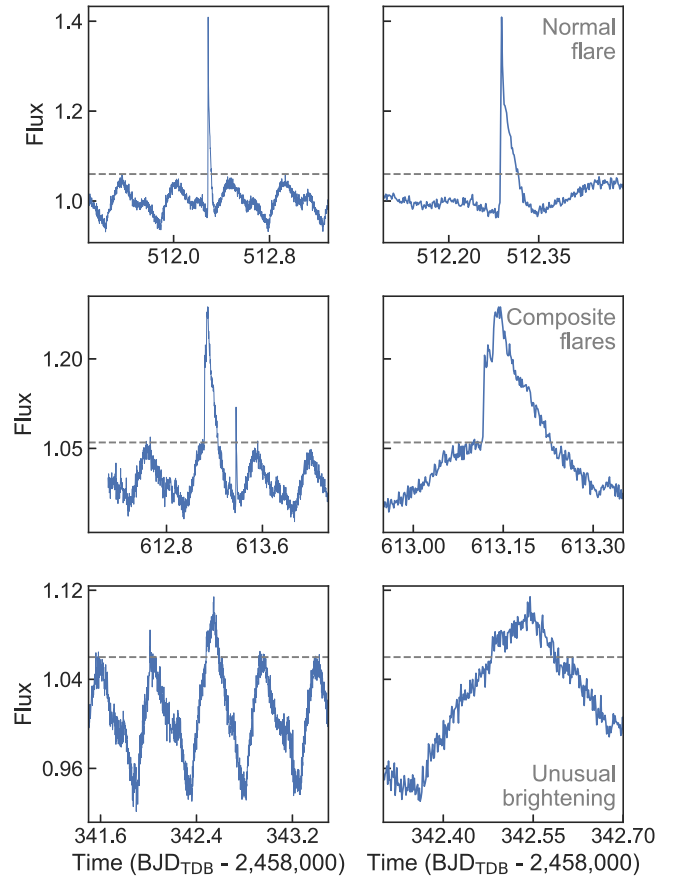


Figure 5. Different flare and brightening profiles of the complex rotators, exemplified by TIC 177309964. Each row shows a global (2 day) and local (5 hr) view of the light-curve brightening. Horizontal dashed lines show the typical nonflare maximum flux value. First row: normal flares are described by the same profiles as main-sequence M dwarfs, suggesting similar origins and processes driving them. Second row: complicated outbursts of flares also resemble those of main-sequence M dwarfs and can be explained as superpositions of sequential flare events (e.g., Günther et al. 2020). Third row: unusual brightenings in the complex rotators often, but not always, occur after large flares and show an amplified version of the usual morphology for a short time.

during Sectors 1 and 2. P_{clouds} is the probability that a given star has a cloud of dust/gas orbiting it at the Keplerian corotation radius. P_{spots} is the probability that a given star has at least one large spot. P_{disk} is the probability that these stars have a dust disk orbiting them at a few stellar radii. P_{misal} is the probability that a given star shows a spin-orbit misalignment between the stellar rotation axis and the dust disk. Finally, P_{geom} is the geometric probability that an existing structure (cloud or disk) falls in the line of sight between the star and the observer.

5.1.1. How Many Young M Dwarfs with Rapid Rotations are Out There?

To first order, we can estimate N_{yMrr} as the number of stars in known open clusters and associations that have effective temperatures below 3900 K and radii below $0.6 R_{\odot}$. For this, we cross-match the TESS short-cadence target lists³⁴ of Sectors 1 and 2 with three young star catalogs:

³⁴ <https://tess.mit.edu/observations/target-lists/> (2020 June 24).

Young M dwarfs in TESS Sectors 1 & 2 (290 in total)

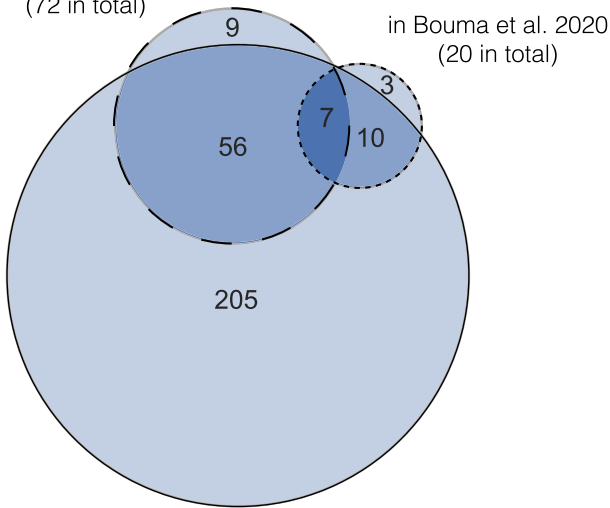
in Feinstein et al. 2020
(72 in total)via `banyan sigma`, Gagné et al. 2018
(278 in total)

Figure 6. Overlap and union of three young star catalogs cross-matched with the TESS short-cadence targets from Sectors 1 and 2. The three catalogs were assembled by Feinstein et al. (2020b), Bouma et al. (2019), and in this work using `banyan sigma` (Gagné et al. 2018).

1. a catalog by Feinstein et al. (2020b), which was assembled through a combination of searching the TESS Guest Investigator proposals and the data from Faherty et al. (2018). All targets were vetted with the `banyan sigma` software (Gagné et al. 2018), and the ones with $\geq 50\%$ probability and available TESS 2 minutes data were included.
2. a catalog by Bouma et al. (2019), collecting targets from numerous literature lists, including members of open clusters, moving groups, and young associations.
3. a catalog we created by matching all TESS short-cadence targets with the `banyan sigma` software (Gagné et al. 2018). The algorithm uses a Bayesian model to predict whether a given target is part of 1 of 27 young associations within 150 pc. The target is identified by its coordinates, proper motion, parallax, distance, and radial velocity measurements, which we retrieve from TICv8 and Gaia DR2.

The results of our cross-matches are shown in Figure 6. We find a total of 290 young M dwarfs from open clusters and young associations. Notably, their real number might be even higher, as new clusters and associations are still being discovered. For example, Gagné et al. (2020) just discovered a new young association at 150 pc, while Castro-Ginard et al. (2020) recently discovered 582 new open clusters in the Galactic disk using Gaia DR2, increasing their total number by 45% (many beyond 150 pc). Additionally, there might still be unidentified M dwarfs among nearby clusters. We thus consider the number of young M dwarfs in TESS Sectors 1 and 2 as $N_{yM} \gtrsim 290$.

To estimate N_{yMrr} from this, we investigate the rotation periods of those 290 M dwarfs using all available TESS data from Sectors 1 through 13. We flag a target as a “young M dwarf with rapid rotation” if we find a rotation period below 2 days using Lomb–

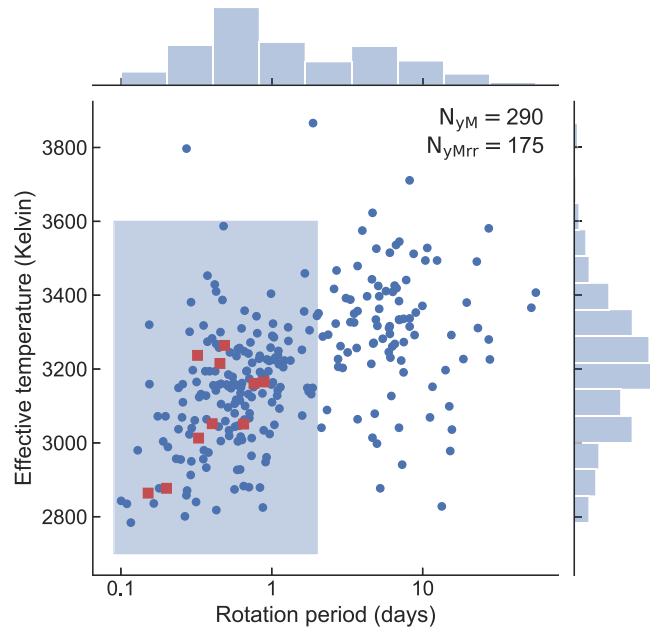


Figure 7. Effective temperatures and rotation periods of the 290 young M-dwarf stars in TESS short cadence from Sectors 1 and 2 (blue circles; N_{yM} : number of young M dwarfs). Out of these, 175 targets show rotation periods shorter than 2 days (blue shaded area; N_{yMrr} : number of young M dwarfs with rapid rotations), comparable to the 10 known complex rotators from this sample (red squares).

Scargle periodograms (Lomb 1976; Scargle 1982). We measure rotation periods for 269 out of the 290 targets, with the remaining 21 targets not showing measurable photometric variability (false-alarm probability > 0.01). This might just be due to low signal-to-noise ratio or the stars might simply be seen pole on; both leave open that they could actually be rapidly rotating. All measured rotation periods and effective temperatures are shown in Figure 7, and we conclude that $N_{yMrr} \gtrsim 175$.

5.1.2. How Many Complex Rotators Should We Expect?

We here put the finding of $N_{yMrr} \gtrsim 175$ into the perspectives of Equations (1) and (2).

Corotating clouds hypothesis—For this hypothesis, we also have to account for (i) P_{clouds} , the probability of clouds of dust/gas being present at the Keplerian corotation radius, R_{cr} , as well as (ii) $P_{\text{geom}}^{\text{CC}}$, the geometric alignment probability of an edge-on alignment with the observer. We can estimate³⁵ $P_{\text{geom}}^{\text{CC}} \approx (R_*/R_{\text{cr}})$, with R_{cr} derived as

$$R_{\text{cr}} = \left(\frac{P_{\text{rot}}}{2\pi} \right)^{\frac{2}{3}} (GM_*)^{\frac{1}{3}}, \quad (3)$$

with the rotation period P_{rot} , gravitational constant G , and stellar mass M_* . For our targets, this yields $R_{\text{cr}} \approx 1 - 6 R_*$ (Table 1), which leads to $P_{\text{geom}}^{\text{CC}} \approx (R_*/R_{\text{cr}}) \approx 0.2 - 1$. Putting all pieces together, we can estimate from Equation (1):

$$\begin{aligned} N_{\text{comp. rot.}}^{\text{CC}} &= N_{yMrr} \cdot P_{\text{clouds}} \cdot P_{\text{geom}}^{\text{CC}} \\ &\approx 175 \cdot P_{\text{clouds}} \cdot (0.2 - 1) \\ &\approx (35 - 175) \cdot P_{\text{clouds}}. \end{aligned} \quad (4)$$

³⁵ Assumes (i) that the clouds are much smaller than the star and (ii) an isotropic distribution of orientations.

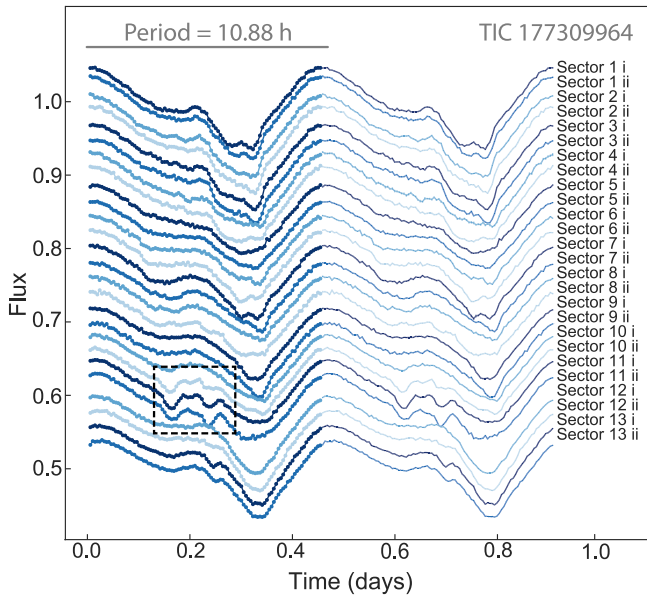


Figure 8. Example of TIC 177309964, illustrating the stability of major photometric features over year-long timescales (TESS orbits from Sectors 1–13, from 2018 July to 2019 July). Each orbit is phase-folded to show two periods of modulation and vertically offset for clarity. Flares have been clipped before plotting. The major features of the modulation remain stable over the full year, while minor features appear and disappear over a few weeks (dashed box).

Given that we found 10 complex rotators in Sectors 1 and 2, this would only require $\lesssim 30\%$ of all rapidly rotating young M dwarf to have material clouds trapped at their Keplerian corotation radius.

Spots and misaligned disk hypothesis—For this hypothesis, we already searched all known young stars in TESS Sectors 1 and 2 for photometric rotation periods and signs of spots and found that, on average, $P_{\text{spots}} \sim 1$ (see above). We estimate the geometric probability $P_{\text{geom}}^{\text{SMD}} \approx (R_*/d)$, where R_* is the stellar radius and $d \approx 5\text{--}15 R_*$ is the outer edge (or gap) of a possible disk (Zhan et al. 2019). This leads to $P_{\text{geom}}^{\text{SMD}} \approx 0.07 - 0.2$ and

$$\begin{aligned} N_{\text{comp. rot.}}^{\text{SMD}} &= N_{\text{yMrr}} \cdot P_{\text{spots}} \cdot P_{\text{disk}} \cdot P_{\text{misal}} \cdot P_{\text{geom}}^{\text{SMD}} \\ &\approx 175 \cdot 1 \cdot P_{\text{disk}} \cdot P_{\text{misal}} \cdot (0.07 - 0.2) \quad (5) \\ &\approx (12 - 35) \cdot P_{\text{disk}} \cdot P_{\text{misal}}. \end{aligned}$$

Considering our 10 complex rotators in Sectors 1 and 2, this would imply that $P_{\text{disk}} \cdot P_{\text{misal}}$ is on the order of 0.3–1. Hence, for this hypothesis to hold true, a large fraction of $\gtrsim 30\%$ of rapidly rotating young M dwarfs would need to have an inner dust disk with a slight spin–orbit misalignment to their rotation axis.

5.2. Time Dependency

The photometric modulations of the complex rotators appear stable over timescales of at least one year (Figure 8 and Figure 9). The complex rotator TIC 177309964 fell into TESS’ continuous viewing zone and was observed for the consecutive Sectors 1–13, spanning an entire year of data from 2018 July 2018 to 2019 July (Figure 8).

We can also see this stability in the examples of TIC 201789285, TIC 206544316, TIC 332517282, and TIC 425933644 (Figure 9) when combining TESS and SSO photometry. The original TESS

data were taken in 2018 August–October, while the SSO observations were taken in 2019 November/December, over one year later. Despite the large time span, the modulation profiles still follow the same pattern and periodicity. All major features remain the same, while only some minor evolution of the morphology is evident in the SSO light curves compared to TESS. In the case of TIC 201789285, it appears that a minor feature has increased in amplitude (near $\text{BJD}_{\text{TDB}} 2,458,795.70$), while another has decreased in amplitude (near $\text{BJD}_{\text{TDB}} 2,458,795.75$).

The stability and longevity of these morphologies are extraordinary. Considering the spots and misaligned disk hypothesis, this is well compatible with the lifetimes of dust disks and the persistence of stellar spots on young M dwarfs. While stellar spots on most stars only last for a few weeks (e.g., on the Sun they last only for three to six rotations Gaiauskas et al. 1983), we have examples like GJ 1243, which had remarkably constant spot modulation over 10 yr observed with Kepler and TESS (Davenport et al. 2020). Notably, GJ 1243 is a member of a young association with an age of around 30–50 Myr and, as such, quite comparable to our complex rotators. Furthermore, a 200 day photometric monitoring campaign of the open cluster Blanco 1 (~ 115 Myr) with the Next Generation Transit Survey (NGTS) suggests that most young M dwarfs display generally stable spot modulation patterns over this baseline, while F, G, and early-K dwarfs show moderate-to-significant evolution in their light-curve morphologies (Gillen et al. 2020).

In contrast, considering the corotating clouds hypothesis, such stability and longevity would seem surprising. The idea does suggest a rather fine-tuning problem with clouds being confined strictly to the corotation radius. Any separating clouds would slowly drift away and slightly alter their orbital period. Even for small drifts, a year-long time span might lead to noticeable changes in the morphologies. This would lead to a certain amount of material away from corotation at any given time, which would blur out the strictly periodic signals over year-long time spans.

5.3. Color Dependency

We obtained a total of nine telescope nights’ worth of SSO observations (Section 2.2) to capture four of the complex rotators in simultaneous multicolor bandpasses. We compare all these light curves with phase-folded TESS observations (taken one year earlier) in Figure 9. Evidently, the sharp-peaked features are more prominent in bluer bandpasses and less expressed in the reddest bandpasses. This matches the expectations from both the corotating clouds and spots and misaligned disk hypotheses: (i) for the corotating clouds hypothesis, the material’s extinction would have to be stronger in the blue, leading to deeper features. (ii) For the spots and misaligned disk hypothesis, the contrast between the stellar surface (~ 3000 K) and a cool spot is stronger in bluer wavelengths. The disk material could be a gray absorber or could have a color dependency, which would add a secondary effect.

Combining TESS data with SSO r -, i -, and g -band observations, our total data span more than one year. We find that the same features are still present in the data at the predicted phases (accounting for uncertainties in the period estimation). There is no doubt that the modulation is still the same and thus stable and long-lived over year-long time spans.

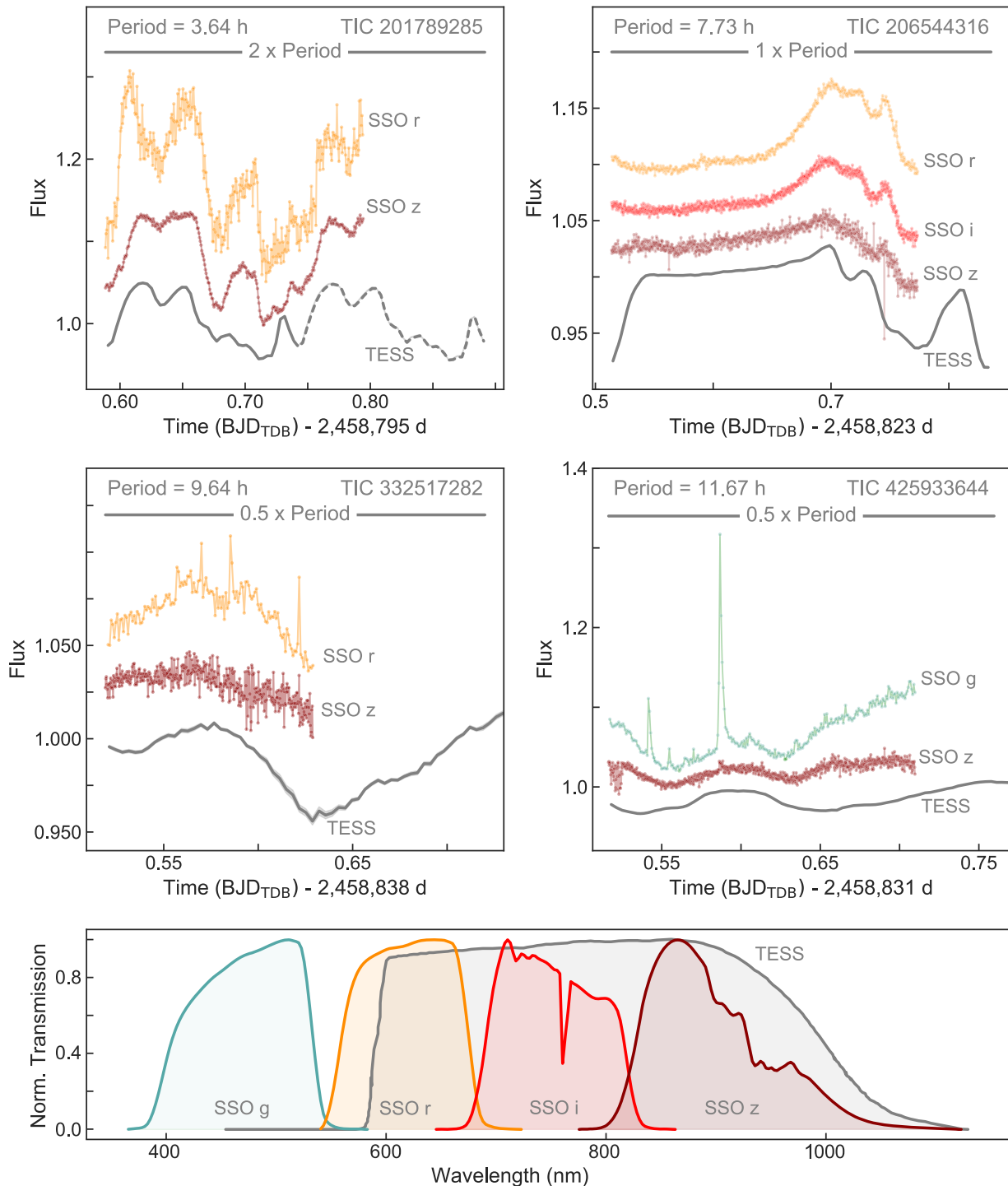


Figure 9. Comparison of multicolor light curves of 4 of the 10 complex rotators: TIC 201789285, TIC 206544316, TIC 332517282, and TIC 425933644. For each target, SSO observations were taken simultaneously in at least two of the g' , r' , i' , and z' bandpasses (shown as green, orange, red and dark-red curves, respectively). For TESS observations, flares have been removed, and light curves are averaged over all available Sectors, binned in 5 minute intervals, and slightly shifted in phase to correct for imprecision in the period measurement (shown as dark-gray curves). The lower panel compares the normalized transmission functions of all respective bandpasses. There is a clear color dependency of the light-curve features visible in the simultaneous SSO observations, with features being much more prominent in bluer bandpasses. Additionally, the general shape and largest features in the SSO light curves are still comparable to the TESS light curve, even though the SSO data were taken about 1 yr later. This suggests that the overall mechanism causing these patterns also causes a color dependency (e.g., spots, nongray dust, or pulsations) and that it is stable over long times.

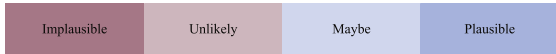
6. Discussion

6.1. Could Spots and Pulsations be Another Hypothesis?

Pulsations on low-mass stars have long been theoretically explored and predicted (e.g., Gabriel 1964; Noels et al. 1974;

Palla & Baraffe 2005; Rodríguez-López et al. 2012, 2014; Rodríguez-López 2019) but, despite observational efforts, have so far proven elusive. In theory, fully nonadiabatic models of M dwarfs suggest that they could excite (i) radial modes, (ii) low-order, low-degree nonradial modes, and (iii) solar-like oscillations

Observations	Spots only	Accreting dust disk	Co-rotating clouds of opaque dust	Co-rotating clouds of warm coronal gas	Dust near the surface	Gas near the surface	Spots and spin-orbit-misaligned dust disk (SSD)	Spots and pulsations	Spots and co-rotating clouds of material
Complex modulation	Implausible (S17, S18, Z19)	Plausible (B16)	Plausible	Plausible (S17, S18)	Unlikely (Z19)	Unlikely (Z19)	Plausible (Z19, this work)	Maybe	Plausible
Narrow-feature amplitudes of several percent	Plausible	Plausible	Plausible	Unlikely (Z19)	Implausible (Z19)	Implausible (Z19)	Plausible (Z19, this work)	Implausible	Maybe
Strict periodicity	Plausible	Implausible (S17, S18, Z19)	Plausible	Plausible (S17, S18)	Maybe (Z19)	Maybe (Z19)	Plausible (Z19, this work)	Implausible	Plausible
Stability & longevity	Plausible	Implausible (S17, S18, Z19)	Maybe	Maybe	Maybe (Z19)	Maybe (Z19)	Plausible (this work)	Maybe	Plausible
Color dependence	Plausible	Maybe	Maybe	Maybe	Maybe	Maybe	Plausible (this work)	Maybe	Plausible
Lack of strong infrared excess	Plausible	Implausible (S17, S18, Z19)	Maybe (S17)	Maybe (S17)	Maybe	Maybe	Maybe (Z19)	Plausible	Maybe
Occurrence rates (10 out of 290 targets)	Plausible	Plausible (C14)	Plausible (this work)	Plausible (this work)	Maybe	Maybe	Maybe (this work)	Maybe	Maybe (this work)
Magnetic activity and frequent flaring	Plausible	Maybe	Maybe	Maybe	Maybe	Maybe	Plausible	Plausible	Plausible
Circumstellar material can be constrained	-	Plausible	Unlikely (Z19)	Maybe	Plausible (Z19)	Plausible (Z19)	Maybe	-	Maybe



C14: Cody et al., 2014
 B16: Bodman et al., 2016
 S17: Stauffer et al., 2017
 S18: Stauffer et al., 2018
 Z19: Zhan et al., 2019

Figure 10. Overview of hypotheses discussed throughout this paper for complex rotators (and scallop shells). All hypotheses are contrasted against observational constraints.

(Rodríguez-López et al. 2012, 2014). This requires the models to be completely convective or have large convective envelopes. This would match the spectral types of all complex rotators and scallop shells, placing the stars beyond the fully convective limit. Periods of the pulsations are predicted to range from 20 minutes to 3 hr, again agreeing with the typical timescales we see for the sharp-peaked features of our targets.

However, the amplitudes of M-dwarf pulsations are expected to be in the range of 1 ppm to 1 ppt, while our targets typically show amplitudes of several percent. The only bypass to this caveat could be a superposition of the effects from spots (creating the smooth, large-amplitude modulations) and synchronous pulsations (creating the sharp-peaked, lower-amplitude features). Yet, this would require spots and pulsations to be synchronized, which seems implausible.

Rodríguez-López et al. (2014) identified the theoretical instability strips of M dwarfs, which resulted in two islands of “instability” in the parameter space. Stars falling into one of these islands would, in theory, be capable of showing pulsations. With the revised and activity-corrected stellar parameters (Section 3), some of the stars fall near the lower island, yet remain outside of it. Again, this makes pulsations seem implausible.

6.2. The Pros and Cons of Various Hypotheses: A Summary

We here briefly summarize the pros and cons of the various hypotheses introduced and scrutinized throughout this paper (see Sections 1 and 6.1 for short overviews). Figure 10 additionally contrasts all observations with all hypotheses, highlighting which aspects can and cannot be explained through a given hypothesis.

Spots only—Pros: Spot modulations can be strictly periodic and stable over many years, even in the presence of differential rotation (e.g., Davenport et al. 2020). The temperature difference between the surface and the spots causes a color dependence, and spots would not cause any infrared excess. Most young stars are spotted and are often accompanied by strong signs of magnetic activity, such as flaring. **Cons:** Spots alone cannot explain the sharp-peaked features (Zhan et al. 2019). However, spots could

still play a major role in combination with other factors (e.g., pulsation or circumstellar material; Sections 6.1 and 6.3).

Accreting dust disk—Pros: Accreting dust disks can lead to the morphologies for dipper/burster stars and occur frequently enough. They might show color dependency depending on the absorption and scattering properties of the material. **Cons:** Accretion is a rather stochastic process, and thus neither strictly periodic nor stable. The dippers and bursters also show strong infrared excess due to the large disks.

Co-rotating clouds of material—Pros: Clouds of material at the Keplerian corotation radius could qualitatively explain sharp features and strict periodicity (Stauffer et al. 2017, 2018). Depending on the material, a color dependency is possible, and small-enough clouds would cause no infrared excess. As young stars are often surrounded by material, they could also occur at high enough rates. **Cons:** If the material is gas, the absorption would likely not be able to explain percentage-scale amplitudes (Zhan et al. 2019). If the material is dust, these clouds are likely not stable at the required distances ($d/R_* \gtrsim 3$; Zhan et al. 2019). Another challenge might be the stability and longevity of the morphology over year-long time spans, i.e., over hundreds of orbital periods. With some parts of the clouds slowly drifting away from corotation, the signals would blur out and evolve, which does not seem to be the case.

Material trapped near the surface—Pros: Material trapped in the magnetic field and bound to the stellar rotation would remain strictly periodic and could survive over many years near the stellar surface ($d/R_* \sim 1$; Zhan et al. 2019). Depending on the material’s properties, a color dependence is possible, and in small amounts, it might not cause any infrared excess. **Cons:** Any material that close in cannot explain the sharp-peaked, percentage-scale amplitudes of the modulation but would instead produce a rather smooth variation similar to spots; this can only be explained by material at larger distances ($d/R_* \gtrsim 3$; Zhan et al. 2019).

Spots and spin-orbit-misaligned dust disks—Pros: The patterns can be strictly periodic and stable over many years. Spots induce a color dependency, and disk material might add

to this effect. There are enough young and rapidly rotating M dwarfs in the sample to explain the high occurrence rates (with caveats; see below). Lastly, the spots are a sign of magnetic activity and agree with the frequent flaring found on the complex rotators and scallop shells. *Cons:* The scenario would require most young M dwarfs to have close-in dust disks with spin-orbit misalignments. There is no obvious formation mechanism that would explain this behavior. Also, the one M dwarf for which we have disk and rotation measurements, Au Mic, does appear coplanar. However, the misalignment does not need not to be very large. A 10° obliquity between the spin and magnetic axes of T Tauri stars is reasonable, based on Zeeman studies and recent work by McGinnis et al. (2020). If the disks are confined by the magnetic field, this slight misalignment could already be enough to mitigate this caveat and cause the observed morphologies. A potential driver for such misalignment might be perturbations from nearby passing stars, either dynamically or through radiation pressure (e.g., Rosotti et al. 2094).

Spots and pulsations—Pros: In theory (qualitatively), a superposition of spots and pulsations could lead to a smooth large-amplitude trend (due to spots) superposed by a sharp-peaked small-amplitude pattern (due to pulsations). Both features can be stable over long times, show color dependencies, a lack of infrared excess, and frequent flaring due to their activity. *Con:* This would require a strict synchronization between rotation and pulsation, which seems implausible. Further, the stars do not lie within any of the theoretical instability islands.

6.3. Toward a Unified Hypothesis: Could It be Spots and Corotating Clouds of Material?

So far, none of the hypotheses stand out as a definite answer, and each comes with limitations. The two most promising hypotheses have their own caveats. On the one hand, the corotating clouds hypothesis, with clouds of gas at the Keplerian corotation radius, could remain stable and allow the required viewing angle, but gas likely cannot explain the large, percentage-scale absorption features. On the other hand, the spots and misaligned disk hypothesis could tick all boxes but have the implicit requirement that a large fraction of rapidly rotating young M dwarfs must have misaligned disks. That said, if the disks are confined by the magnetic field, a small misalignment of $\sim 10^\circ$ seems not to be uncommon (McGinnis et al. 2020) and could have been induced by nearby passing stars (e.g., Rosotti et al. 2094).

Rapidly rotating young M dwarfs are known to be magnetically active and generally show high spot coverage rates. Spots alone were ruled out easily, but what was not explored so far is: How much can spots explain?

The superposition of smooth, large-amplitude spot modulations and sharp, sudden features from transits of corotating clouds of gas could represent a unified hypothesis (spots and corotating clouds). This explanation could expand the corotating clouds hypothesis by requiring only a minimal amount of circumstellar material to cause the overall morphology, making gas clouds a more plausible candidate. It would also mitigate the occurrence rate caveats that challenge the spots and misaligned disk hypothesis.

6.4. Toy Models

We developed simplified forward models for the three most promising ideas, the (i) corotating clouds, (ii) spots and misaligned disk, and (iii) spots and corotating clouds hypotheses. We took the TESS light curve of TIC 201789285 as an example and tried to imitate its morphology as closely as possible while keeping the models simple, using a hybrid of statistical inference and manual parameter selection. We model the star as a fine grid in spherical coordinates. The rotation axis of the star is left as a free parameter, and a quadratic limb-darkening effect is applied to each cell based on its orientation relative to the observer.

For the spots and misaligned disk hypothesis, we model spots with four parameters: two angles describing the location on the star, its size, and its temperature. The disk is parameterized by its inner and outer radius, inclination, and opacity. The observed flux is computed for each grid cell by integrating the Planck function across the TESS bandpass, accounting for geometric effects, spots, and the disk. We then try to mimic the TESS light curve of TIC 201789285 by choosing a simple model with three cold spots and a fully opaque disk, optimizing their parameters using nested sampling via *dynesty* (Speagle 2020).

For the corotating clouds and the spots and corotating clouds hypotheses, we model the torus of clouds as a series of orbiting spheres whose orbital period matches the rotational period of the star. For this, we used the *processing* package (<https://processing.org/>) to draw the model and count the flux in each pixel. We then manually evaluated different scenarios of spots and sparse to dense tori of clouds.

We find that all three toy models can replicate the typical morphology of complex rotators (Figure A3). Additionally, spots as drivers for an underlying large-amplitude modulation can explain a large portion of the signal, easing the constraints on circumstellar material.

6.5. What Can TESS Short Cadence Do for Us?

The TESS complex rotators were all found in short-cadence (2 minutes) observations. In contrast, the K2 scallop shells were discovered using 30 minute cadence. However, the longer cadence means that the data are limited by the Nyquist frequency, and numerous harmonics will be missed in the frequency spectrum (see Figure 1). We tested whether we would have discovered the complex rotators in the same way from TESS long-cadence (30 minutes) observations, by extracting light curves directly from the full-frame images (FFI). For this, we used a TESS FFI photometry pipeline based on the one developed by Pál (2012). It is designed to extract photometry of faint stars in crowded fields ($\text{TESS-mag} > 15$) by combining difference and aperture photometry. We selected nearby stars from the Gaia DR2 catalog that could contaminate the target's light curve and applied a principal component analysis (PCA) detrending.

We find that the complex rotator morphologies are most apparent in the 2 minute cadence data and that many might have been missed due to their sharp-peaked features being blurred out in 30 minute cadence data (Figure 11). The 2 minute data will thus be the best source to search for more complex rotators throughout Sectors 1–23. With the start of the TESS extended mission, 20 s cadence data will be enabled.

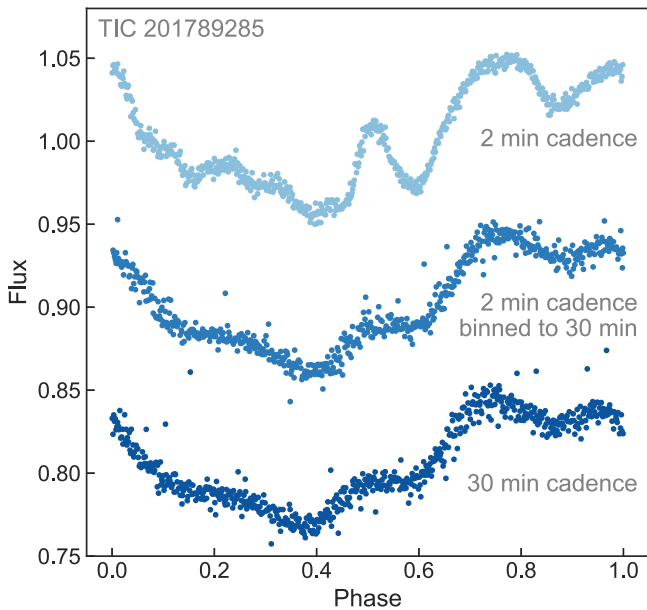


Figure 11. Comparison of TESS 2 and 30 minute light curves on the example of TIC 201789285, showing that the complex rotators’ sharp-peaked features are blurred in long-cadence data. TESS’ 2 minutes and upcoming 20 s observing cadences are hence ideal for detecting more of these targets.

Additionally, both the original TESS sectors as well as the K2 fields will be revisited. Reobserving complex rotators and scallop shells with such short cadence could greatly increase our sensitivity to the sharpest features.

6.6. Implications for Exoplanet Systems

We know, thanks to Kepler and other missions, that, on average, each early- to mid-M dwarf has at least one small exoplanet (Dressing & Charbonneau 2015). All complex rotators and scallop shells are young mid-M dwarfs (most around 10–45 Myr), raising the question of how the effects causing their morphology might impact young, recently formed exoplanets. After all, for the corotating clouds, spots and misaligned disk, and spots and corotating clouds hypotheses, occurrence rates suggest that most young M dwarfs would go through the same processes, we just cannot see their morphologies (Section 5.1).

At these ages, most processes driving planet formation have likely been concluded. Terrestrial planet formation is thought to be completed after at most 10–30 Myr, regardless of the driving processes (e.g., Chambers 2010). In particular, gas-giant planets around mid- to late M dwarfs are rare; even if they formed around any complex rotators, they require a substantial amount of gas in the protoplanetary disk to be present at the late stage of their formation, yielding formation time spans of less than 10 Myr (the maximum lifetime of gas disks; e.g., D’Angelo et al. 2010).

The material in question for causing the complex morphologies, however, is likely much closer to the star (near 3–10 stellar radii) than any forming or migrating exoplanets. Exoplanet systems hosted by mid-M dwarfs are widely studied, and if the effects at play for complex rotators are indeed ubiquitous at early ages, they seem to not have caused a strong effect on their planets.

If the spots and misaligned disk hypothesis were correct, more than half of all young M dwarfs would have a slight spin-orbit misalignment between their rotation axis and remnant

dust disk. An interesting question is whether this would imply the protoplanetary disk to also be misaligned. However, there are currently no strong signs that a large fraction of exoplanets forming around M dwarfs have spin-orbit misalignments. Limited data suggest there to be a wide variety. For example, Au Mic b is proven to be aligned (e.g., Hirano et al. 2020a), the TRAPPIST-1 system might be slightly misaligned (Hirano et al. 2020b), and GJ 436 b is inclined (Knutson et al. 2011; Bourrier et al. 2017).

7. Conclusion

Recently, at least one new distinct morphology class of young stars has been discovered in white-light photometry from Kepler/K2 and TESS (Stauffer et al. 2016, 2017; Zhan et al. 2019), adding to the seven classes established by Cody et al. (2014; which include dippers and bursters). Here, we added three puzzle pieces to unveil the physical nature of these complex rotators and probe whether several hypotheses could hold true given these new observational constraints.

The tested hypotheses include spots only, accreting dust disks, corotating clouds of material, magnetically constrained material, spots and a spin-orbit-misaligned disk, and spots and pulsations. We particularly focused on the corotating clouds and spots and misaligned disk hypotheses, as others are ruled out more easily.

First, we investigated if their occurrence rates make sense in light of the total number of rapidly rotating young M dwarfs in the given field of view. We find that TESS Sectors 1 and 2 harbor at least 175 young M dwarfs with rotation periods below 2 days, rendering the finding of 10 complex rotators plausible. However, for both hypotheses, this comes with a caveat. For the corotating clouds hypothesis to work, this would mean that almost every such star must have clouds of dust/gas trapped at the Keplerian corotation radius. For the spots and misaligned disk hypothesis to work, this would imply that a large fraction of these stars must have an inner disk and show a spin-orbit-misalignment. If the latter holds true, it could have consequences for exoplanet systems around mid-to-late M dwarfs, which might have formed under the same conditions.

Second, we studied the longevity of these features over one year, and find that they remain remarkably stable over these time spans. While the major features of the complex rotators remain unchanged, we find evidence for additional small features building up and decaying over a few weeks. In the corotating clouds hypothesis, this would imply subtle changes in the dust/gas cloud structures. In the spots and misaligned disks hypothesis, this can very likely be caused by smaller spots appearing and disappearing, major spots changing size, or spots wandering along the surface.

Third, we probe the color dependency of the complex rotators’ photometric features. We indeed find the expected behavior predicted by both the corotating clouds and the spots and misaligned disk hypotheses. The features are more pronounced in bluer wavelengths, which could be explained by either chromatic absorption by the circumstellar material or the smaller spot-to-star brightness contrast in the red/infrared.

All new clues to the case—occurrence rates, longevity, and color dependency—could in principle match any of the hypotheses shown in Figure 2. It is well possible that the truth will lie somewhere between these hypotheses. Rapidly rotating young M dwarfs are known to be magnetically active, so the final answer will likely have contributions from both spots and

circumstellar material, leading to their complex photometric morphologies.

We thank John Stauffer and Andrew Collier-Cameron for fruitful discussions about complex rotators and scallops, John Bredall and Benjamin J. Shappee for providing their custom detrended light curve of the dipper star RY Lup, Gerald Handler for his insights on pulsation, and Victor See for discussions about M-dwarf activity.

Funding for the TESS mission is provided by NASA’s Science Mission directorate. Resources supporting this work were provided by the NASA High-End Computing (HEC) Program through the NASA Advanced Supercomputing (NAS) Division at Ames Research Center for the production of the SPOC data products. This paper includes data collected by the TESS mission, which are publicly available from the Mikulski Archive for Space Telescopes (MAST). STScI is operated by the Association of Universities for Research in Astronomy, Inc. under NASA contract NAS 5-26555. The research leading to these results has received funding from the European Research Council under the European Union’s Seventh Framework Programme (FP/2007–2013) ERC Grant Agreement n° 336480, from the European Union’s Horizon 2020 research and innovation program (grant agreement n° 803193/BEBOP), from the ARC grant for Concerted Research Actions financed by the Wallonia-Brussels Federation, from the Balzan Prize Foundation, from F.R.S-FNRS (Research Project ID T010920F), from the Simons Foundation, from the MERAC foundation, and from STFC, under grant number ST/S00193X/1. This work has made use of data from the European Space Agency (ESA) mission Gaia (<https://www.cosmos.esa.int/gaia>), processed by the Gaia Data Processing and Analysis Consortium (DPAC, <https://www.cosmos.esa.int/web/gaia/dpac/consortium>). Funding for the DPAC has been provided by national institutions, in particular the institutions participating in the Gaia Multilateral Agreement.

M.N.G. acknowledges support from MIT’s Kavli Institute as a Juan Carlos Torres Fellow and from the European Space Agency (ESA) as an ESA Research Fellow. K.O. and B.S. acknowledge support from the Hungarian National Research, Development and Innovation Office grant OTKA K131508.

B.S. is supported by the ÚNKP-19-3 New National Excellence Program of the Ministry for Innovation and Technology. J.N.W. and B.V.R. thank the Heising-Simons Foundation for support. A.D.F. acknowledges the support from the National Science Foundation Graduate Research Fellowship Program under grant No. (DGE-1746045). Any opinions, findings, and conclusions or recommendations expressed in this material are those of the author(s) and do not necessarily reflect the views of the National Science Foundation. E.G. gratefully acknowledges support from the David and Claudia Harding Foundation in the form of a Winton Exoplanet Fellowship. M.G. is F.R.S.-FNRS Senior Research Associate. B.-O.D. acknowledges support from the Swiss National Science Foundation (PP00P2-163967). J.M.D.K. gratefully acknowledges funding from the Deutsche Forschungsgemeinschaft (DFG, German Research Foundation) through an Emmy Noether Research Group (grant number KR4801/1-1), the DFG Sachbeihilfe (grant number KR4801/2-1), and the SFB 881 “The Milky Way System” (subproject B2), as well as from the European Research Council (ERC) under the European Union’s Horizon 2020 research and innovation program via the ERC Starting Grant MUSTANG (grant agreement number 714907).

Facilities: TESS, SSO, ANU.

Software: `numpy` (van der Walt et al. 2011), `matplotlib` (Hunter 2007), `pandas` (McKinney 2010), `casutools` (Irwin et al. 2004), `banyan sigma` (Gagné et al. 2018), SPOC pipeline (Jenkins et al. 2016), `stella` (Feinstein et al. 2020a, 2020b), `everest` (Luger et al. 2016, 2018), `processing` (<https://processing.org/>).

Appendix

In the following, we provide additional illustrations and summaries of our analysis. Figure A1 provides an overview of all available TESS light curves of the 10 original complex rotators. Figure A2 shows the SED fits for revising their stellar parameters. Figure A3 displays light-curve morphologies created via toy models for the three most plausible hypotheses. Finally, Table A1 summarises all SSO Observations.

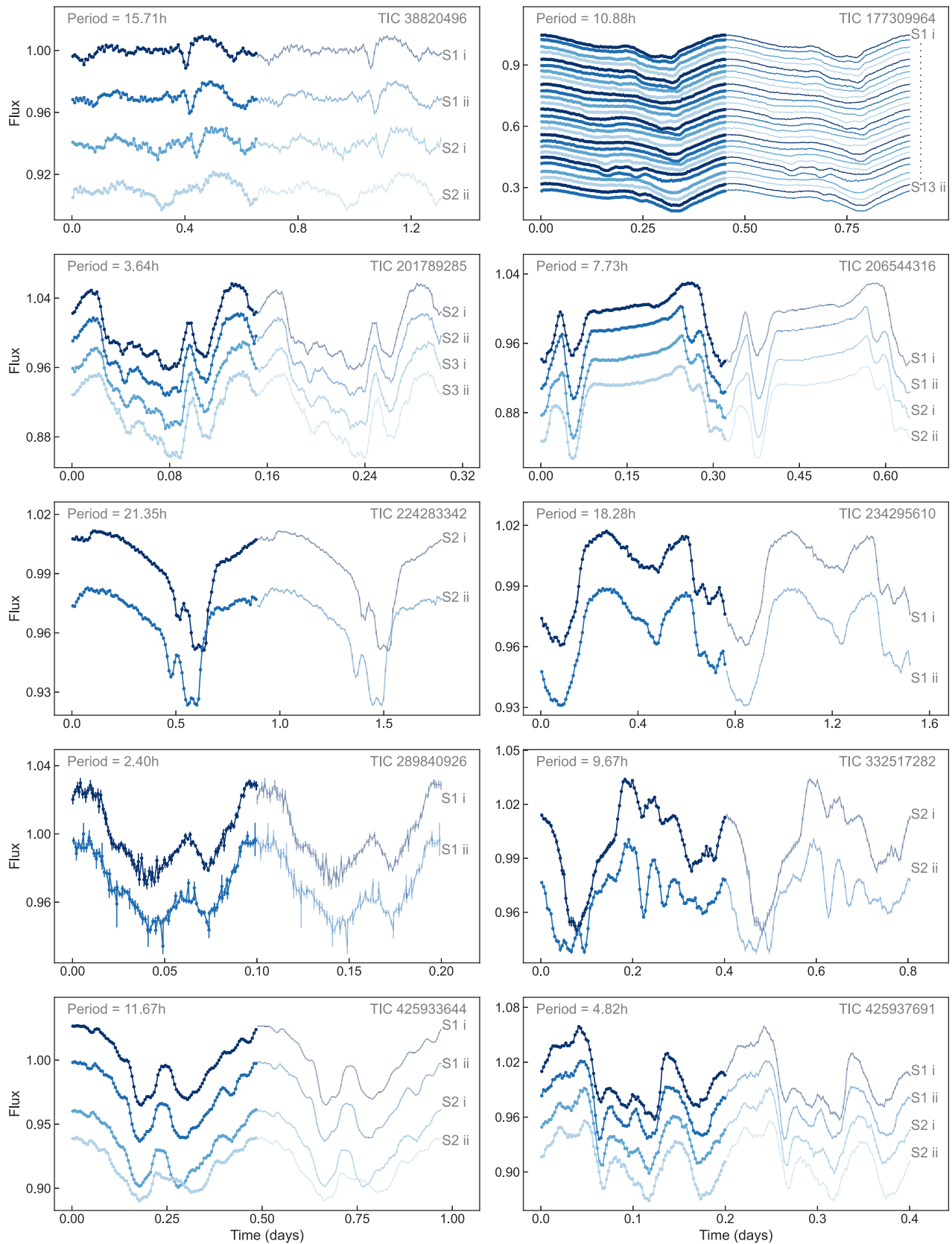


Figure A1. All available TESS light curves of young M dwarfs with complex photometric variability, spanning multiple Sectors of TESS observations. Each light curve shows the data of one TESS orbit (14 days of observations) phase-folded onto the rotational period of each star, with, e.g., “S1 i” denoting the first orbit of Sector 1 and “S13 ii” denoting the second orbit of Sector 13. Flares have been removed prior to phase-folding and plotting. All complex rotators’ features show remarkable stability and longevity over many weeks to a year (at least). See also Figure 8 for a closer view of TIC 17730996.

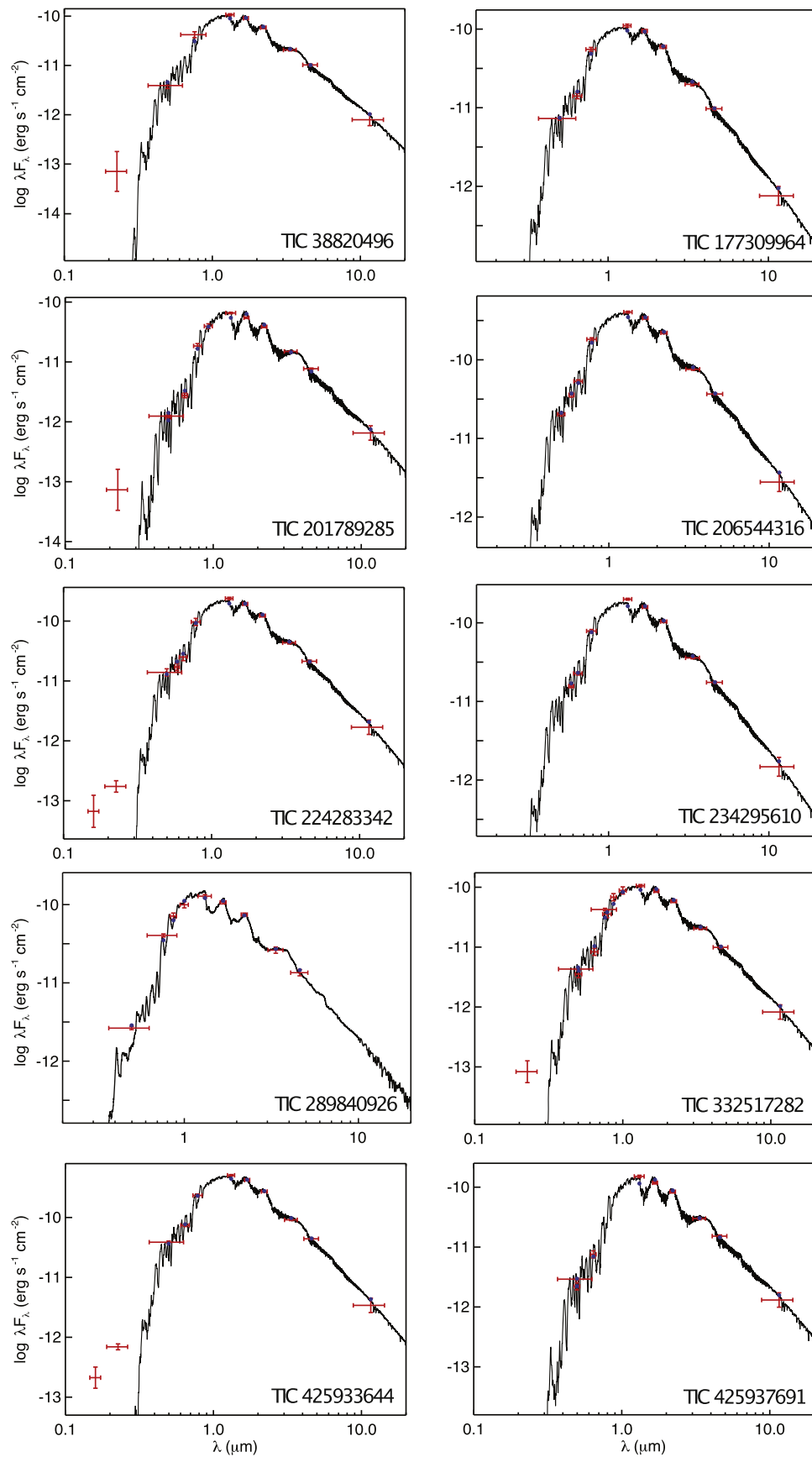


Figure A2. All SED fits for the 10 complex rotators. The results are used to determine the stars' apparent effective temperatures and radii. The near-UV and blue optical excesses for some targets are consistent with chromospheric activity, another indicator of strong magnetic activity for these stars. Notably, no infrared excesses are seen.

Table A1
Summary of all SSO Observations for 4 of the 10 Complex Rotators

Target	Telescope	Date	Filter	Exposure (s)	On Sky Duration (h)	# Images
TIC 201789285	SSO/Jo	20191107	r'	35	4.93	392
	SSO/Europa	20191107	z'	40	4.94	357
TIC 206544316	SSO/Jo	20191205	z'	10	6.23	1096
	SSO/Europa	20191205	i'	10	6.23	1101
	SSO/Ganymede	20191205	r'	30	6.22	560
TIC 332517282	SSO/Jo	20191220	r'	60	2.60	135
	SSO/Europa	20191220	z'	12	2.63	431
TIC 425933644	SSO/Callisto	20191213	g'	50	4.62	278
	SSO/Europa	20191213	z'	10	4.64	827

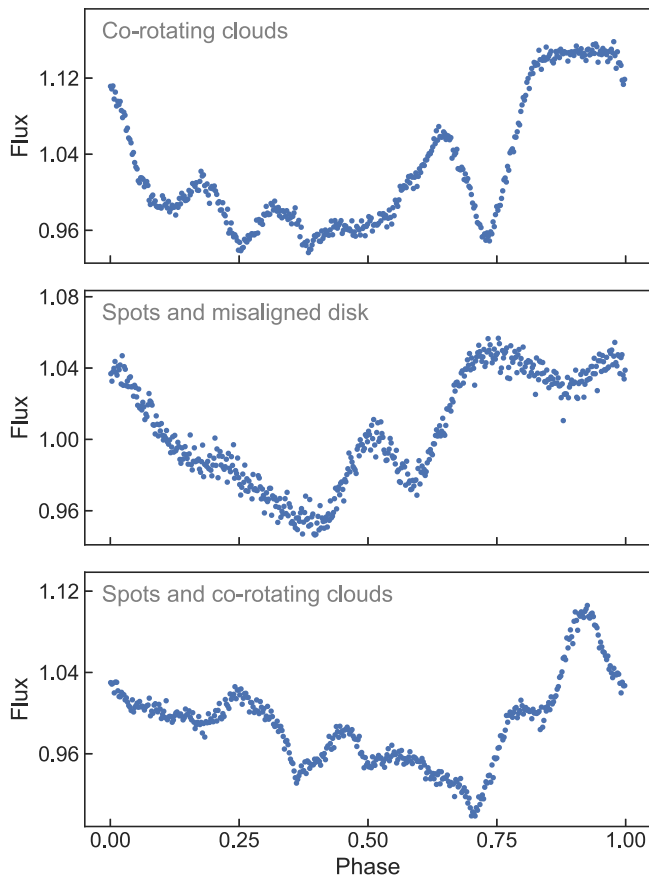


Figure A3. Toy models of a complex rotator derived from three different hypotheses, aiming to replicate the morphology of TIC 201789285.

ORCID iDs

Maximilian N. Günther <https://orcid.org/0000-0002-3164-9086>
 David A. Berardo <https://orcid.org/0000-0001-6298-412X>
 Elsa Ducrot <https://orcid.org/0000-0002-7008-6888>
 Catriona A. Murray <https://orcid.org/0000-0001-8504-5862>
 Keivan G. Stassun <https://orcid.org/0000-0002-3481-9052>
 Katalin Olah <https://orcid.org/0000-0003-3669-7201>
 L. G. Bouma <https://orcid.org/0000-0002-0514-5538>
 Saul Rappaport <https://orcid.org/0000-0003-3182-5569>

Joshua N. Winn <https://orcid.org/0000-0002-4265-047X>
 Adina D. Feinstein <https://orcid.org/0000-0002-9464-8101>
 Elisabeth C. Matthews <https://orcid.org/0000-0003-0593-1560>
 Daniel Sebastian <https://orcid.org/0000-0002-2214-9258>
 Benjamin V. Rackham <https://orcid.org/0000-0002-3627-1676>
 Bálint Seli <https://orcid.org/0000-0002-3658-2175>
 Amaury H. M. J. Triaud <https://orcid.org/0000-0002-5510-8751>
 Edward Gillen <https://orcid.org/0000-0003-2851-3070>
 Alan M. Levine <https://orcid.org/0000-0001-8172-0453>
 Brice-Olivier Demory <https://orcid.org/0000-0002-9355-5165>
 Michaël Gillon <https://orcid.org/0000-0003-1462-7739>
 Didier Queloz <https://orcid.org/0000-0002-3012-0316>
 George R. Ricker <https://orcid.org/0000-0003-2058-6662>
 Roland K. Vanderspek <https://orcid.org/0000-0001-6763-6562>
 Sara Seager <https://orcid.org/0000-0002-6892-6948>
 David W. Latham <https://orcid.org/0000-0001-9911-7388>
 Jon M. Jenkins <https://orcid.org/0000-0002-4715-9460>
 C. E. Brasseur <https://orcid.org/0000-0002-9314-960X>
 Knicole D. Colón <https://orcid.org/0000-0001-8020-7121>
 Tansu Daylan <https://orcid.org/0000-0002-6939-9211>
 Laetitia Delrez <https://orcid.org/0000-0001-6108-4808>
 Michael Fausnaugh <https://orcid.org/0000-0002-9113-7162>
 Lionel J. Garcia <https://orcid.org/0000-0002-4296-2246>
 Rahul Jayaraman <https://orcid.org/0000-0002-7778-3117>
 Emmanuel Jehin <https://orcid.org/0000-0001-8923-488X>
 Martti H. Kristiansen <https://orcid.org/0000-0002-2607-138X>
 J. M. Diederik Kruijssen <https://orcid.org/0000-0002-8804-0212>
 Peter Pihlmann Pedersen <https://orcid.org/0000-0002-5220-609X>
 Francisco J. Pozuelos <https://orcid.org/0000-0003-1572-7707>
 Joseph E. Rodriguez <https://orcid.org/0000-0001-8812-0565>
 Bill Wohler <https://orcid.org/0000-0002-5402-9613>
 Zhuchang Zhan <https://orcid.org/0000-0002-4142-1800>

References

Alencar, S. H., Teixeira, P. S., Guimarães, M. M., et al. 2010, *A&A*, 519, A88
 Ansdell, M., Gaidos, E., Williams, J. P., et al. 2016, *MNRAS*, 462, 101
 Baraffe, I., Homeier, D., Allard, F., & Chabrier, G. 2015, *A&A*, 577, A42
 Bayliss, D., Zhou, G., Penev, K., et al. 2013, *AJ*, 146, 113
 Benz, A. O., & Güdel, M. 2010, *ARA&A*, 48, 241
 Bodman, E. H. L., Quillen, A. C., Ansdell, M., et al. 2016, *MNRAS*, 470, 202

- Bouma, L. G., Hartman, J. D., Bhatti, W., Winn, J. N., & Bakos, G. A. 2019, *ApJSS*, **245**, 13
- Bouma, L. G., Winn, J. N., Ricker, G. R., et al. 2020, *AJ*, **160**, 86
- Bourrier, V., Lovis, C., Beust, H., et al. 2017, *Natur*, **553**, 477
- Bredall, J. W., Shappee, B. J., Gaidos, E., et al. 2020, *MNRAS*, **496**, 3257
- Browning, M. K. 2008, *ApJ*, **676**, 1262
- Burdanov, A., Delrez, L., Gillon, M., & Jehin, E. 2018, *Handbook of Exoplanets* (Berlin: Springer), 130
- Castro-Ginard, A., Jordi, C., Luri, X., et al. 2020, *A&A*, **635**, A45
- Chambers, J. 2010, in *Exoplanets*, ed. S. Seager (Tucson, AZ: Univ. of Arizona Press), 297
- Cody, A. M., Stauffer, J., Baglin, A., et al. 2014, *AJ*, **147**, 2014
- D'Angelo, G., Durisen, R. H., & Lissauer, J. J. 2010, in *Exoplanets*, ed. S. Seager (Tucson, AZ: Univ. of Arizona Press), 319
- Davenport, J. R. A., Hebb, L., & Hawley, S. L. 2015, *ApJ*, **806**, 212
- Davenport, J. R. A., Mendoza, G. T., & Hawley, S. L. 2020, *AJ*, **160**, 36
- Delrez, L., Gillon, M., Queloz, D., et al. 2018, *Proc. SPIE*, **10700**, 1070011
- Dopita, M., Hart, J., McGregor, P., et al. 2007, *Ap&SS*, **310**, 255
- Doyle, J. G., Shetye, J., Antonova, A. E., et al. 2018, *MNRAS*, **475**, 2842
- Doyle, L., Ramsay, G., & Doyle, J. G. 2020, *MNRAS*, **494**, 3596
- Doyle, L., Ramsay, G., Doyle, J. G., & Wu, K. 2019, *MNRAS*, **489**, 437
- Dressing, C. D., & Charbonneau, D. 2015, *ApJ*, **807**, 45
- Faherty, J. K., Bochanski, J. J., Gagné, J., et al. 2018, *ApJ*, **863**, 91
- Feinstein, A., Montet, B., & Ansdell, M. 2020a, *JOSS*, **5**, 2347
- Feinstein, A. D., Montet, B. T., Ansdell, M., et al. 2020b, *AJ*, **160**, 219
- Gabriel, M. 1964, *AnAp*, **27**, 141
- Gagné, J., David, T. J., Mamajek, E. E., et al. 2020, *ApJ*, **903**, 96
- Gagné, J., Mamajek, E. E., Malo, L., et al. 2018, *ApJ*, **856**, 23
- Gaia Collaboration, Brown, A. G. A., Vallenari, A., et al. 2018, *A&A*, **616**, A1
- Gaiauskas, V., Harvey, K. L., Harvey, J. W., & Zwaan, C. 1983, *ApJ*, **265**, 1056
- Gillen, E., Briegal, J. T., Hodgkin, S. T., et al. 2020, *MNRAS*, **492**, 1008
- Gillon, M. 2018, *NatAs*, **2**, 344
- Günther, M. N., & Daylan, T. 2021, *ApJS*, **254**, 13
- Günther, M. N., Zhan, Z., Seager, S., et al. 2020, *AJ*, **159**, 60
- Hirano, T., Gaidos, E., Winn, J. N., et al. 2020a, *ApJL*, **890**, L27
- Hirano, T., Krishnamurthy, V., Gaidos, E., et al. 2020b, *ApJL*, **899**, L13
- Hunter, J. D. 2007, *CSE*, **9**, 90
- Irwin, M. J., Lewis, J., Hodgkin, S., et al. 2004, *Proc. SPIE*, **5493**, 411
- Jenkins, J. M. 2002, *ApJ*, **575**, 493
- Jenkins, J. M. 2017, Kepler Science Document, KSCI-19081-002
- Jenkins, J. M., Chandrasekaran, H., McCauliff, S. D., et al. 2010, *Proc. SPIE*, **7740**, 77400D
- Jenkins, J. M., Twicken, J. D., McCauliff, S., et al. 2016, *Proc. SPIE*, **9913**, 99133E
- Knutson, H. A., Madhusudhan, N., Cowan, N. B., et al. 2011, *ApJ*, **735**, 27
- Kővári, Z., & Bartus, J. 1997, *A&A*, **323**, 801
- Lomb, N. R. 1976, *Ap&SS*, **39**, 447
- Lloyd, R. O. P., Shkolnik, E. L., France, K., Wood, B. E., & Youngblood, A. 2020, *RNAAS*, **4**, 119
- Luger, R., Agol, E., Kruse, E., et al. 2016, *AJ*, **152**, 100
- Luger, R., Kruse, E., Foreman-Mackey, D., et al. 2018, *AJ*, **156**, 99
- McGinnis, P., Bouvier, J., & Gallet, F. 2020, *MNRAS*, **497**, 2142
- McKinney, W. 2010, in *Proc. of the 9th Python in Science Conf.*, ed. S. van der Walt & J. Millman (Austin, TX: SciPy), 56
- Moffatt, H. K. 1978, *Magnetic field generation in electrically conducting fluids* (Cambridge: Cambridge Univ. Press)
- Morales-Calderón, M., Stauffer, J. R., Hillenbrand, L. A., et al. 2011, *ApJ*, **733**, 50
- Muirhead, P. S., Dressing, C. D., Mann, A. W., et al. 2018, *AJ*, **155**, 180
- Murray, C. A., Delrez, L., Pedersen, P. P., et al. 2020, *MNRAS*, **495**, 2446
- Newton, E. R., Irwin, J., Charbonneau, D., et al. 2017, *ApJ*, **834**, 85
- Noels, A., Boury, A., Scudlare, R., & Gabriel, M. 1974, *A&A*, **31**, 185
- Notsu, Y., Shibayama, T., Machara, H., et al. 2013, *ApJ*, **771**, 127
- Pál, A. 2012, *MNRAS*, **421**, 1825
- Palla, F., & Baraffe, I. 2005, *A&A*, **432**, 57
- Parker, E. N. 1979, *Cosmical Magnetic Fields Their Origin and their Activity* (Oxford: Clarendon Press)
- Rappaport, S., Swift, J., Levine, A., et al. 2014, *ApJ*, **788**, 114
- Rodríguez-López, C. 2019, *FrASS*, **6**, 76
- Rodríguez-López, C., MacDonald, J., Amado, P. J., Moya, A., & Mullan, D. 2014, *MNRAS*, **438**, 2371
- Rodríguez-López, C., Macdonald, J., & Moya, A. 2012, *MNRAS Letters*, **419**, 44
- Roettenbacher, R. M., & Vida, K. 2018, *ApJ*, **868**, 3
- Rosotti, G. P., Dale, J. E., Dale, M. D. J., et al. 2014, *MNRAS*, **441**, 2094
- Scargle, J. D. 1982, *ApJ*, **263**, 835
- Smith, J. C., Stumpe, M. C., Van Cleve, J. E., et al. 2012, *PASP*, **124**, 1000
- Speagle, J. S. 2020, *MNRAS*, **493**, 3132
- Stassun, K. G., Kratter, K. M., Scholz, A., & Dupuy, T. J. 2012, *ApJ*, **756**, 47
- Stassun, K. G., Oelkers, R. J., Pepper, J., et al. 2018, *AJ*, **156**, 102
- Stauffer, J., Cameron, A. C., Jardine, M., et al. 2017, *AJ*, **153**, 152
- Stauffer, J., Cody, A. M., Rebull, L., et al. 2016, *AJ*, **151**, 60
- Stauffer, J., Rebull, L., David, T., et al. 2018, *AJ*, **155**, 63
- Strassmeier, K. G., Granzer, T., Mallonn, M., Weber, M., & Weingrill, J. 2017, *A&A*, **597**, A55
- Stumpe, M. C., Smith, J. C., Catanzarite, J. H., et al. 2014, *PASP*, **126**, 100
- van der Walt, S., Colbert, S. C., & Varoquaux, G. 2011, *CSE*, **13**, 22
- Vida, K., Kriskovics, L., Oláh, K., et al. 2016, *A&A*, **590**, A11
- West, A. A., Weisenburger, K. L., Irwin, J., et al. 2015, *ApJ*, **812**, 3
- Wolter, U., Robrade, J., Schmitt, J. H. M. M., & Ness, J. U. 2007, *A&A*, **478**, 11
- Wright, N. J., Newton, E. R., Williams, P. K. G., Drake, J. J., & Yadav, R. K. 2018, *MNRAS*, **479**, 2351
- Yu, L., Winn, J. N., Gillon, M., et al. 2015, *ApJ*, **812**, 48
- Zhan, Z., Günther, M. N., Rappaport, S., et al. 2019, *ApJ*, **876**, 127
- Zhang, Y., Liu, J., & Zhang, H. 2008, *SoPh*, **247**, 39